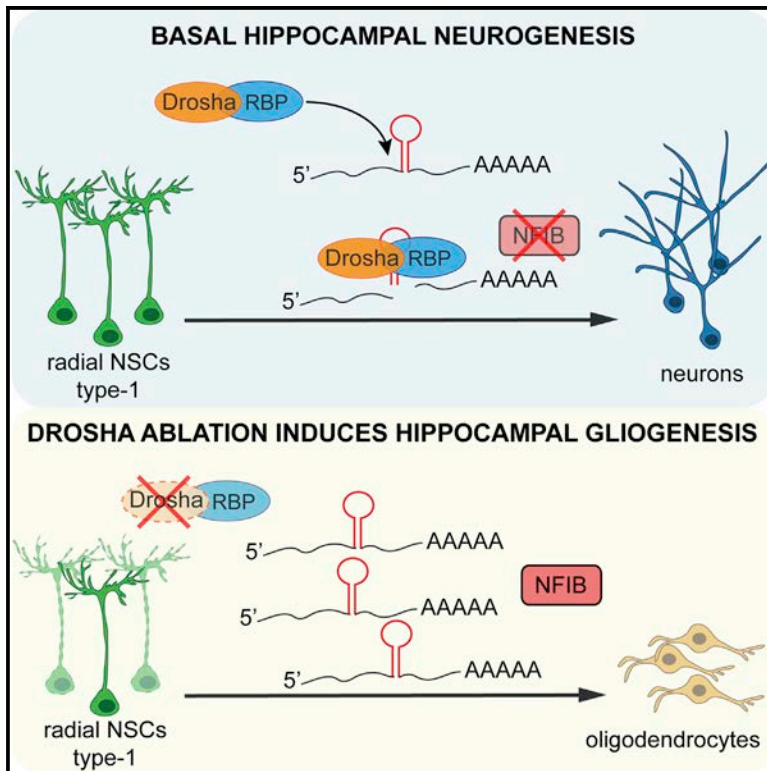


Multipotency of Adult Hippocampal NSCs In Vivo Is Restricted by Drosha/NFIB

Graphical Abstract



Authors

Chiara Rolando, Andrea Erni, Alice Grison, ..., Thomas Wegleiter, Sebastian Jessberger, Verdon Taylor

Correspondence

verdon.taylor@unibas.ch

In Brief

Rolando et al. investigated the function of the RNaseIII Drosha in the regulation of adult hippocampal stem cell maintenance and differentiation. They found that Drosha directly inhibits the expression of the transcription factor NFIB through a miRNA-independent mechanism, thereby permitting neurogenesis and preventing oligodendrocyte fate commitment.

Highlights

- Drosha regulates adult hippocampal stem cell maintenance
- Drosha inhibits oligodendrocytic differentiation of adult stem cells
- Drosha targets NFIB mRNA hairpin to inhibit expression and enable neurogenesis
- NFIB expression induces oligodendrocytic fate in adult hippocampal stem cells

Multipotency of Adult Hippocampal NSCs In Vivo Is Restricted by Drosha/NFIB

Chiara Rolando,^{1,4} Andrea Erni,^{1,4} Alice Grison,¹ Robert Beattie,¹ Anna Engler,¹ Paul J. Gokhale,² Marta Milo,² Thomas Wegleiter,³ Sebastian Jessberger,³ and Verdon Taylor^{1,5,*}

¹Department of Biomedicine, University of Basel, Mattenstrasse 28, 4058 Basel, Switzerland

²Department of Biomedical Science, University of Sheffield, Western Bank, Sheffield S10 2TN, UK

³Brain Research Institute, Faculty of Medicine and Science, University of Zurich, 8057 Zurich, Switzerland

⁴Co-first author

⁵Lead Contact

*Correspondence: verdon.taylor@unibas.ch

<http://dx.doi.org/10.1016/j.stem.2016.07.003>

SUMMARY

Adult neural stem cells (NSCs) are defined by their inherent capacity to self-renew and give rise to neurons, astrocytes, and oligodendrocytes. In vivo, however, hippocampal NSCs do not generate oligodendrocytes for reasons that have remained enigmatic. Here, we report that deletion of Drosha in adult dentate gyrus NSCs activates oligodendrogenesis and reduces neurogenesis at the expense of gliogenesis. We further find that Drosha directly targets NFIB to repress its expression independently of Dicer and microRNAs. Knockdown of NFIB in Drosha-deficient hippocampal NSCs restores neurogenesis, suggesting that the Drosha/NFIB mechanism robustly prevents oligodendrocyte fate acquisition in vivo. Taken together, our findings establish that adult hippocampal NSCs inherently possess multilineage potential but that Drosha functions as a molecular barrier preventing oligodendrogenesis.

INTRODUCTION

Somatic stem cells can generate progeny throughout life, but their fates are usually restricted, and they generate specific cell types in their respective tissue. Active adult neural stem cells (NSCs) are present in two regions of the brain: the subventricular zone (SVZ) of the lateral ventricles and the subgranule zone of the hippocampal dentate gyrus (DG) (Ihrie and Alvarez-Buylla, 2011; Kriegstein and Alvarez-Buylla, 2009). Although both SVZ and DG NSCs are multipotent, they generate specific neuron types. SVZ NSCs become fate restricted during embryonic development and generate multiple interneuron populations from topological locations in the lateral ventricle wall (Merkle et al., 2007). DG NSCs produce only granule neurons, which contribute to cognition, and loss or dormancy of stem cells during aging can result in psychological disorders and disease (Kronenberg et al., 2003; Petrus et al., 2009; Santarelli et al., 2003; Steiner et al., 2008). Whereas SVZ NSCs make a significant number of oligodendrocytes (Hack et al., 2004; Menn et al., 2006), new oligodendro-

cytes are normally not produced in the adult DG (Bonaguidi et al., 2011; Encinas et al., 2011; Lugert et al., 2010). In vitro, DG NSCs also rarely produce oligodendrocytes, although oligodendrocytic differentiation can be induced by their co-culture with neurons and in vivo by inactivation of the Neurofibromin 1 gene or reprogramming with the transcription factor Ascl1 (Braun et al., 2015; Jessberger et al., 2008; Song et al., 2002; Suh et al., 2007; Sun et al., 2015). This suggests an intrinsic and niche-independent fate restriction of DG NSCs that prevents oligodendrocyte formation. How DG NSC potency and particularly oligodendrocytic fate are restricted remains unclear.

Drosha is part of the microRNA (miRNA) microprocessor (Ha and Kim, 2014). However, Drosha can also cleave and directly destabilize mRNAs encoding proteins that regulate cell fate decisions (Chong et al., 2010; Han et al., 2009; Knuckles et al., 2012; Macias et al., 2012). During embryonic development, Drosha maintains embryonic NSCs in an undifferentiated, multipotent state by targeting and cleaving the mRNA of the proneural factor Ngn2 (Knuckles et al., 2012). This non-canonical function of Drosha does not require Dicer or miRNAs, and is a rapid mechanism for fate regulation.

Here, we examined how Drosha is involved in the regulation of DG NSC fate. We found that Drosha controls DG NSC maintenance and cell fate acquisition through a non-canonical regulation of the transcription factor nuclear factor IB (NFIB). We show that NFIB is required for the oligodendrocytic commitment by DG NSCs and propose that Drosha promotes neurogenesis and inhibits oligodendrocyte fate acquisition in the hippocampus by repressing NFIB.

RESULTS

Drosha Deletion from Adult DG NSCs Impairs Neurogenesis

NSCs in the DG of the adult mouse are Notch dependent and express the Notch target *Hes5* (Lugert et al., 2010, 2012). Drosha is expressed by most cells in the DG, including GFAP⁺ and Hes5⁺ radial NSCs (Figures S1A and S1B). To address the functions of Drosha in neurogenic DG NSCs, we treated *Hes5::CreER*^{T2} mice carrying floxed *Drosha* (Drosha cKO) or wild-type (wt) *Drosha* (ctrl) alleles with tamoxifen (TAM) and followed cell fate by lineage tracing (*Rosa26-CAG::EGFP*) (Figures 1A and S1A) (Lugert et al., 2012). Twenty-one days after TAM administration, Hes5⁺

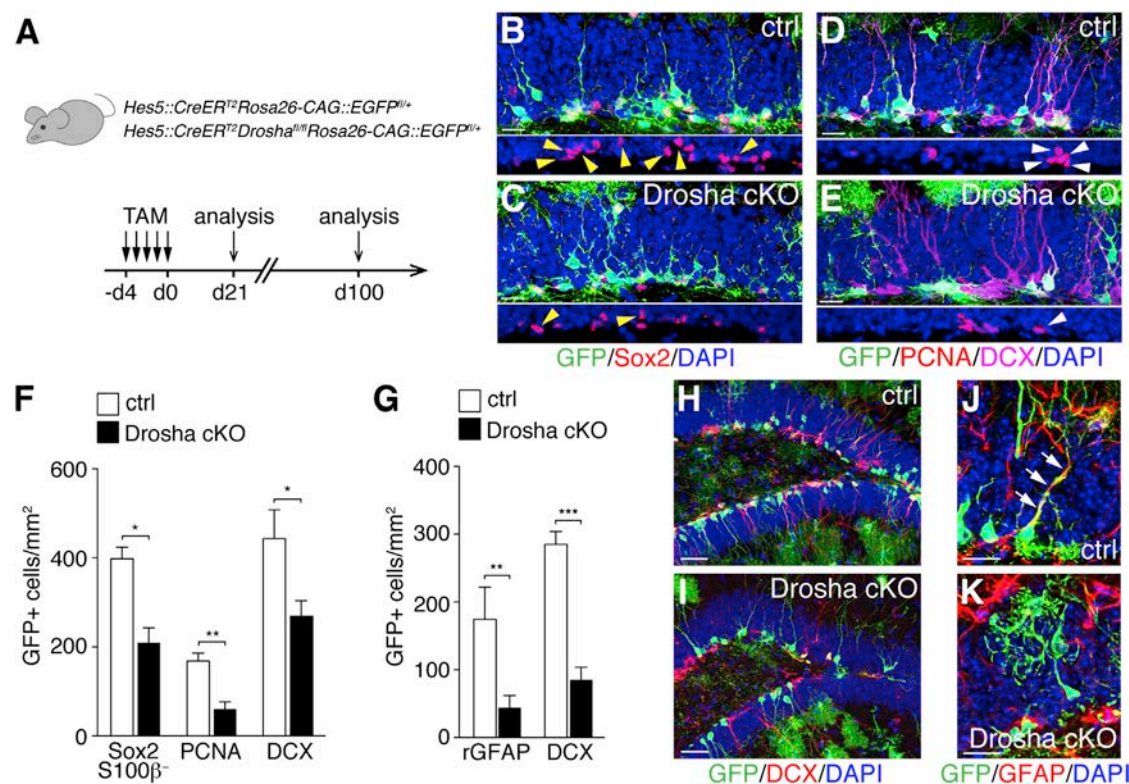


Figure 1. Drosha Deletion from Adult DG NSCs Impairs Neurogenesis In Vivo

(A) TAM induction regime and genotypes of *Hes5::CreER^{T2}* mice.

(B and C) GFP⁺Sox2⁺ NSCs (yellow arrowheads) in the DG of control (B) and Drosha cKO (C) animals at day 21.

(D and E) Proliferating cells (PCNA⁺; white arrowheads) and DCX⁺ neuroblasts in control (D) and Drosha cKO (E) animals at day 21.

(F) Quantification of GFP⁺Sox2⁺S100β⁻ NSCs, proliferating GFP⁺PCNA⁺ progenitors and newly generated neuroblasts GFP⁺DCX⁺ in Drosha cKO and control animals at day 21 (control, n = 5; Drosha cKO, n = 5). Two-sided Student's t test: *p < 0.05, **p < 0.01.

(G) Quantification of radial GFP⁺GFAP⁺ NSCs and DCX⁺ neuroblasts in Drosha cKO and control animals at day 100 (control, n = 5; Drosha cKO, n = 5). Two-sided Student's t test: **p < 0.01, ***p < 0.001.

(H and I) GFP⁺DCX⁺ neuroblasts in control (H) and Drosha cKO (I) animals at day 100.

(J and K) GFP⁺GFAP⁺ cells in control (J) and Drosha cKO (K) animals at day 100 (arrows in J; GFAP⁺ radial process).

Data are mean ± SEM. The scale bars represent 20 μm in (B)–(E), (J), and (K) and 50 μm in (H) and (I). See also Figure S1 and Table S1.

NSCs and their progeny were Drosha deficient and generated fewer cells compared with controls (Figures S1B–S1D). Furthermore, the number of radial GFAP⁺, Sox2⁺, and mitotic (PCNA⁺) NSC/progenitors and neuroblasts (DCX⁺) was reduced in Drosha cKO animals (Figures 1B–1F and S1E). Decreased neurogenesis persisted in Drosha cKO animals at 100 days, and the reduction in newborn neurons (GFP⁺NeuN⁺) was accompanied by an increase in S100β⁺ parenchymal astrocytes compared with controls (Figures 1G–1I and S1F–S1J). In addition, GFAP⁺ putative radial NSCs were lost in Drosha cKO animals (Figures 1G, 1J, and 1K). Together these data suggest that Drosha is required for NSC maintenance and promotes neurogenesis in the DG at the expense of gliogenesis.

Quiescent DG NSCs activate, proliferate, and produce neuroblasts in response to seizures (Hüttmann et al., 2003; Sierra et al., 2015; Steiner et al., 2008). We addressed whether NSC-like progenitors remain in the Drosha cKO and can still respond to activating stimuli. We administered epileptogenic kainic acid (KA) to induce seizures in *Hes5::CreER^{T2}* Drosha cKO and control mice 21 days after TAM induction (Figure S1K). Whereas KA induced

proliferation and an increase in neuroblasts in control animals (Figures S1L and S1M), neither proliferation (PCNA⁺) nor neuroblast (DCX⁺) production was increased following KA treatment of Drosha cKO mice (Figures S1L and S1N). This suggests that Drosha cKO diminishes the DG NSC pool and compromises progenitor reactivation.

Drosha cKO Induces Oligodendrocyte Commitment of NSCs

To examine whether Drosha controls neurogenesis by acting on quiescent NSCs, we ablated *Drosha* specifically in radial GFAP⁺ NSCs by stereotactic infection with adenoviruses expressing Cre-recombinase under the control of the *gfap* promoter (adeno-*gfap::Cre*) (Figure S2A) (Merkle et al., 2007). Six days post-infection (dpi), most GFP-labeled, adeno-*gfap::Cre*-infected cells in the subgranular zone in control mice were GFAP⁺ putative radial NSCs (Figures S2B–S2D). Twenty-one days post-infection, adeno-*gfap::Cre*-infected NSCs had generated mitotic (PCNA⁺) progenitors and neuroblasts (DCX⁺) in control animals, but Sox2⁺ and PCNA⁺ progenitors were almost absent, and

newly formed neuroblasts were reduced in Drosha cKO animals (Figures 2A–2E). Therefore, Drosha cKO DG NSCs lose stem cell potential, demonstrating that Drosha is essential for NSC maintenance and neurogenesis.

DG NSCs normally generate glutamatergic granule neurons and astrocytes but not oligodendrocytes (Bonaguidi et al., 2011). Following adeno-*gfap::Cre*-mediated Drosha cKO, a significant number of the newborn cells expressed Olig2 and Sox10, markers of oligodendrocyte progenitor cells (OPCs) (Figures 2D–2G). Similarly, we observed newly generated Sox10⁺, Olig2⁺, and NG2⁺ OPCs in *Hes5::CreER^{T2}* Drosha cKO animals (Figures S2E–S2G). Thus, Drosha cKO induces a fate switch in DG NSCs to oligodendrocytes.

We performed clonal analysis of *Hes5::CreER^{T2}* Drosha cKO NSC fate. Two days after low-dose TAM induction, labeled NSCs were sparse in the DG (mean distance between clones = $184.3 \pm 17.2 \mu\text{m}$; Figures S2H and S2I). Twenty-one days post-TAM, 6 of the 41 clones examined in Drosha cKO animals contained OPCs but none in the controls (Figures 2H, 2I, S2J, and S2K). Interestingly, 1 clone contained neuroblasts, astrocytes, and oligodendrocytes, indicating tri-lineage potential of Drosha cKO NSC in vivo (Figure 2H).

We addressed whether Drosha controls oligodendrocyte production from mitotic GFAP⁺ stem/progenitor cells. We infected dividing cells in the DG with a Cre-expressing retrovirus. We did not see oligodendrocyte formation in the Drosha cKO after retro-Cre virus infection, and active progenitors continued to generate neuroblasts (Figures S2L and S2M). These data suggest that Drosha deletion induces a fate shift in the quiescent NSC pool to oligodendrocyte production but not in active NSC/progenitors.

Dicer regulates miRNA maturation downstream of Drosha. To investigate whether Drosha regulates oligodendrocyte commitment of NSCs via miRNAs, we deleted Dicer (Dicer cKO) from radial DG NSCs with the adeno-*gfap::Cre* virus (Figure S2A). Dicer cKO did not affect the number of Sox2⁺ progenitors (data not shown) and caused a minor decrease in neuroblasts, consistent with the role of Dicer in neuronal survival and maturation (Figures 2G, S2N, and S2O) (Davis et al., 2008). Unlike Drosha cKO, Dicer cKO did not induce oligodendrocytic differentiation of DG NSCs (ctrl versus Dicer cKO, $p = 0.56$; Figures 2F and 2G). Therefore, Drosha but not Dicer inhibits oligodendrocyte differentiation of adult DG NSCs in vivo, indicating that the mechanism of induced fate switching caused by the loss of Drosha does not primarily involve miRNAs.

Drosha cKO DG NSCs Produce Oligodendrocytes In Vitro

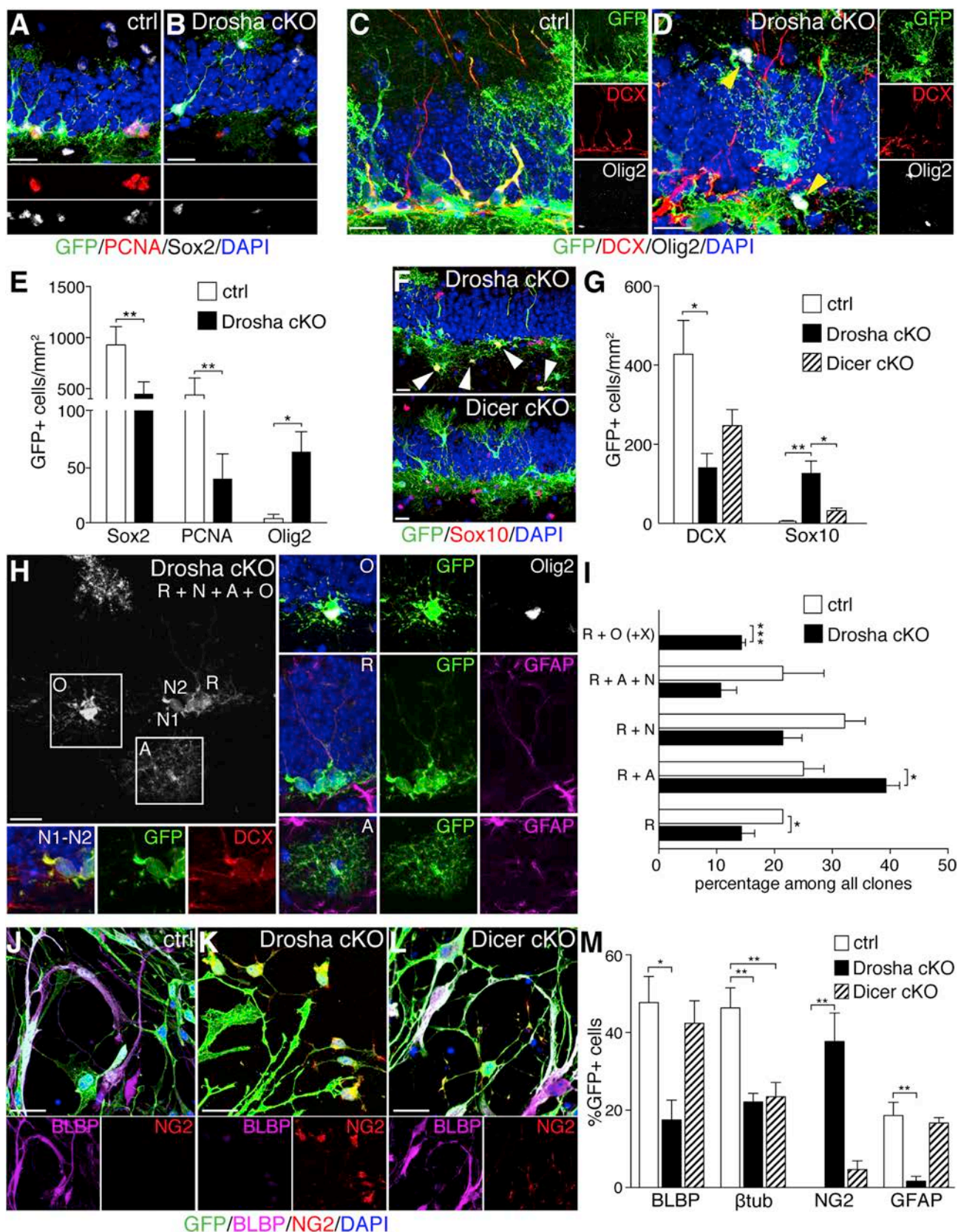
To investigate the mechanisms of Drosha-regulated NSC fate acquisition, we generated a self-renewing DG NSC culture system that recapitulates in vivo features of neurogenesis including expression of the progenitor markers Sox2 and BLBP (Figure S2P). Upon growth factor removal (–FGF2/–EGF), DG NSCs differentiated into neurons and astrocytes but not oligodendrocytes, indicating conserved intrinsic cell fate restriction (Figure S2Q; data not shown) (Bonaguidi et al., 2011; Lugert et al., 2010). We cultured DG NSCs from adult *Drosha^{fl/fl}*, *Dicer^{fl/fl}*, and *Drosha^{wt/wt}Dicer^{wt/wt}* (control) animals that carried the *Rosa26-CAG::EGFP* Cre reporter. Following adeno-Cre viral

transduction, we investigated the effects of Drosha and Dicer cKO (Figures S2R and S2S). Two days post-infection, BLBP⁺ progenitors were reduced in the Drosha cKO compared with control and Dicer cKO cultures, similar to the reduction in progenitors after Drosha ablation in vivo (Figures 2J–2M). Both differentiated Drosha cKO and Dicer cKO NSCs generated fewer neurons in vitro (Figures 2M and S2T–S2V). However, we observed an increase in apoptotic cells (cleaved Caspase3⁺) in the Dicer cKO cultures compared with Drosha cKO and control, confirming that Dicer is crucial for neuronal survival and providing an explanation for the reduction in neurons in its absence (Figure S2W). Drosha cKO induced an increase in NG2⁺ OPCs in the cultures and this at the expense of neuron and astrocyte production (Figures 2K, 2M, and S2X). Dicer cKO induced a slight but not significant increase in NG2⁺ OPCs in the cultures (ctrl versus Dicer cKO, $p = 0.27$; Figures 2L and 2M). Hence, DG NSCs retain a cell-intrinsic bias against oligodendrocyte differentiation in vitro, and Drosha controls this fate decision. We sorted Drosha cKO, Dicer cKO, and control DG NSCs 48 hr after adeno-Cre virus infection in vitro and determined the expression profiles of 381 miRNAs by microarray. Two hundred sixty miRNAs were detected in control DG NSCs (mean Ct values < 32), and their levels were not significantly changed 48 hr after Drosha cKO ($R^2 = 0.81$; Figure S2Y), even though the phenotypes were well established by this time. Dicer cKO resulted in moderate changes in miRNA levels after 48 hr ($R^2 = 0.66$; Figure S2Z), although Dicer cKO NSCs did not display an obvious phenotype at this time. Hence, Drosha cKO did not cause major global changes in miRNA levels, and any changes were less than in Dicer cKO DG NSCs. These data support that the mechanism of Drosha suppression of oligodendrocyte production by DG NSCs is independent of Dicer and miRNAs.

Drosha Binds and Cleaves the NFIB mRNA Regulating Expression

Drosha can bind and cleave hairpin loops in mRNAs (Chong et al., 2010; Han et al., 2009; Knuckles et al., 2012; Macias et al., 2012). In silico analysis (EvoFold) (Pedersen et al., 2006) revealed two evolutionarily conserved hairpins in the mRNA of NFIB, a short 20-base hairpin in the 5' UTR (5' UTR HP) and a longer hairpin of 83 bases in the 3' UTR (3' UTR HP) (Figure 3A). NFIB plays roles in the development of glial cells and myelin tracts (Barry et al., 2008; Deneen et al., 2006; Harris et al., 2015; Kang et al., 2012; Steele-Perkins et al., 2005). To examine whether Drosha binds directly to NFIB mRNA in DG NSCs, we performed cross-linked immunoprecipitation (CLIP) for endogenous Drosha protein and examined the bound RNAs (Figures S3A and S3B). NFIB mRNA cross-linked immunoprecipitated with Drosha from DG NSCs, as did the known target DGCR8 mRNA (Figures 3B and S3B) (Han et al., 2009; Knuckles et al., 2012).

In order to address whether either of the two NFIB mRNA hairpins convey Drosha association, we placed the 5' UTR HP and 3' UTR HP into the SV40 3' UTR downstream of the *Renilla* Luciferase (rLuc) coding region of the psiCheck reporter vector (Figure 3C). We expressed 5' UTR HP and 3' UTR HP containing rLuc mRNAs in N2a cells and performed CLIP to address binding by Drosha. Both the 5' UTR HP and 3' UTR HP of NFIB bound to Drosha more efficiently than the SV40 3' UTR sequence alone



(legend on next page)

(Figure 3D). These data suggest that both NFIB mRNA hairpins are bound by Drosha.

We evaluated whether Drosha cleaves the NFIB hairpins by in vitro processing assays (Figure 3E) (Lee and Kim, 2007). Incubation of in vitro transcribed NFIB 3' UTR RNA with purified Flag-tagged Drosha resulted in cleavage and generation of RNA fragments (Figure 3F). NFIB 5' UTR HP was not cleaved in vitro, suggesting that, although bound, it is not processed by Drosha (Figure S3C). We assessed whether fragmented NFIB mRNAs were present in DG NSCs in vivo by 5' rapid amplification of cDNA ends (5'RACE). Multiple NFIB mRNAs fragmented in the vicinity of the 3' UTR HP were detected in wt NSCs (Figure S3D). Fragmented NFIB transcripts were not detected in Drosha cKO NSCs, supporting that NFIB mRNA fragmentation at the 3' UTR HP is dependent on Drosha (Figure S3D). Sequencing and mapping of 48 independent clones of the NFIB 5'RACE fragments supported the in vitro processing analysis (Figures 3F and S3D). The multiple fragmented RNA species suggest that either Drosha processing of the 3' UTR HP is not as accurate as its processing of a pri-miRNA RNA or additional ribonucleases may be associated with the Drosha complex, and these cleave the RNAs further. We analyzed changes in NFIB RNA fragmentation in sorted NSCs following Drosha cKO compared with control by qRT-PCR over the 3' UTR HP. Drosha cKO increased the relative levels of non-cleaved NFIB transcripts, confirming the Drosha-dependent destabilization of NFIB RNAs in vivo (Figure 3G).

To evaluate whether Drosha affects translation of NFIB 3' UTR HP mRNAs, we performed Luciferase assays in cultured adult DG NSCs (Figure S3E). Drosha cKO increased Luciferase activity of an NFIB 3' UTR HP containing synthetic mRNA (Figure S3F). Surprisingly, Dicer cKO also increased translation of the NFIB 3' UTR HP containing Luciferase mRNA by an unknown mechanism, indicating that under these experimental conditions, Dicer can also regulate NFIB 3' UTR HP containing mRNAs.

Drosha interaction with hairpins in mRNAs can result in destabilization of the transcripts (Han et al., 2009; Knuckles et al., 2012). We isolated *Hes5::CreER^{T2}* Drosha cKO and *Hes5::CreER^{T2}* control (Drosha^{wt/wt}) DG NSCs by fluorescence-activated cell sorting (FACS) based on GFP expression from the Cre-activated *Rosa26-CAG::EGFP* locus following acute induction with TAM (Figure S3G). Drosha mRNA levels were reduced in Drosha cKO cells compared with controls (Figure S3G). Interestingly, NFIB mRNA levels were increased in Drosha cKO NSCs, suggesting that Drosha suppresses NFIB mRNA expression in

DG NSCs in vivo (Figure S3G). As cultured DG NSCs retain Drosha function and blockade of oligodendrocyte differentiation, we speculated that Drosha-dependent regulation of NFIB should also be present in vitro. We infected DG NSCs in vitro with adeno-Cre virus and isolated Drosha cKO and control NSCs by FACS 2 dpi (Figure S3H). NFIB and Sox10 mRNA levels were increased in cultured Drosha cKO but not in Dicer cKO NSCs (Figure S3H). Therefore, Drosha regulates NFIB mRNA levels in DG NSCs in vivo and in vitro.

Drosha cKO-Induced Oligodendrocytic Differentiation Depends on NFIB

We addressed whether NFIB is sufficient to drive oligodendrogenesis from adult DG NSCs. Overexpressed NFIB increased Sox10⁺ and NG2⁺ OPCs in DG NSC cultures and had a negative impact on neurogenesis (Figures 4A and S4A–S4E). Therefore, expression of NFIB is sufficient to induce programming of DG NSCs to oligodendrocytes. We addressed whether NFIB is required for the Drosha cKO-induced oligodendrocyte differentiation of NSCs. We ablated Drosha from DG NSCs in vitro with adeno-Cre viruses and simultaneously prevented NFIB mRNA accumulation by knockdown using specific endoribonuclease-prepared small interfering RNAs (esiRNAs) (Figure 4B). Twenty-four hours after esiRNA transfection, NFIB mRNAs were undetectable in DG NSCs compared with cells transfected with a control rLuc esiRNA (Figure S4F). Neither esiRNA rLuc nor esiRNA NFIB expression affected the differentiation of control DG NSCs (Figures 4C, 4D, S4G, and S4H). As expected, most Drosha cKO NSCs transfected with the esiRNA rLuc differentiated into NG2⁺ OPCs (Figures 4C and 4E). In contrast, NFIB knockdown reduced NFIB expression and decreased oligodendrocytic differentiation of Drosha cKO cells (Figures 4C and 4F). Like their control counterparts, NFIB knockdown Drosha cKO NSCs adopted a neuronal fate or remained as progenitors (Figures 4G and 4H). Thus, Drosha negatively regulates DG NSC differentiation toward an oligodendrocytic fate by suppressing NFIB mRNA levels (Figure S4I). Upon Drosha cKO, inhibition of NFIB is released, and an oligodendrocytic differentiation program is activated (Figure S4J).

DISCUSSION

Adult NSC identity is orchestrated by complex regulatory gene networks and neurogenic niche microenvironments. Post-transcriptional modifications add an additional level of

Figure 2. Drosha Deletion from DG NSCs Induces Oligodendrocyte Fate Commitment

(A and B) GFP⁺Sox2⁺ progenitors and GFP⁺PCNA⁺ mitotic cells in control (A) and Drosha cKO (B) animals at day 21 post-adeno-*gfap::Cre* virus infection. (C and D) GFP⁺DCX⁺ neuroblasts and GFP⁺Olig2⁺ oligodendrocytes in control (C) and Drosha cKO (D) animals at day 21. (E) Quantification of GFP⁺Sox2⁺, GFP⁺PCNA⁺ progenitors and GFP⁺Olig2⁺ oligodendrocytes in control and Drosha cKO day 21 after adeno-*gfap::Cre* virus infection (control, n = 3; Drosha cKO, n = 3) Two-sided Student's t test: *p < 0.05, **p < 0.01. (F) GFP⁺Sox10⁺ oligodendrocytes in Drosha cKO and Dicer cKO animals. (G) Quantification of GFP⁺DCX⁺ neuroblasts and GFP⁺Sox10⁺ oligodendrocytes upon Drosha cKO and Dicer cKO (control, n = 3; Drosha cKO, n = 3; Dicer cKO, n = 3). ANOVA with Bonferroni post hoc test: *p < 0.05, **p < 0.01. (H) Tripotent clone derived from a single Drosha cKO NSC. A, astrocyte; N, neuron; O, oligodendrocyte; R, radial NSC. (I) Quantification of clone composition in control and Drosha cKO (control clones, n = 28; Drosha cKO clones, n = 41). Two-sided Student's t test: *p < 0.05, ***p < 0.001. (J–L) GFP⁺BLBP⁺ and GFP⁺NG2⁺ expression in cultured control (J), Drosha cKO (K), and Dicer cKO (L) NSCs 2 dpi with adeno-Cre virus. (M) Quantification of neural lineage marker expression by adeno-Cre-infected (GFP⁺) control, Drosha cKO, and Dicer cKO NSCs 2 dpi (n = 4). Kruskal-Wallis with Dunn post hoc test: *p < 0.05, **p < 0.01. Data are mean ± SEM. The scale bars represent 20 μm. See also Figure S2 and Tables S2 and S3.

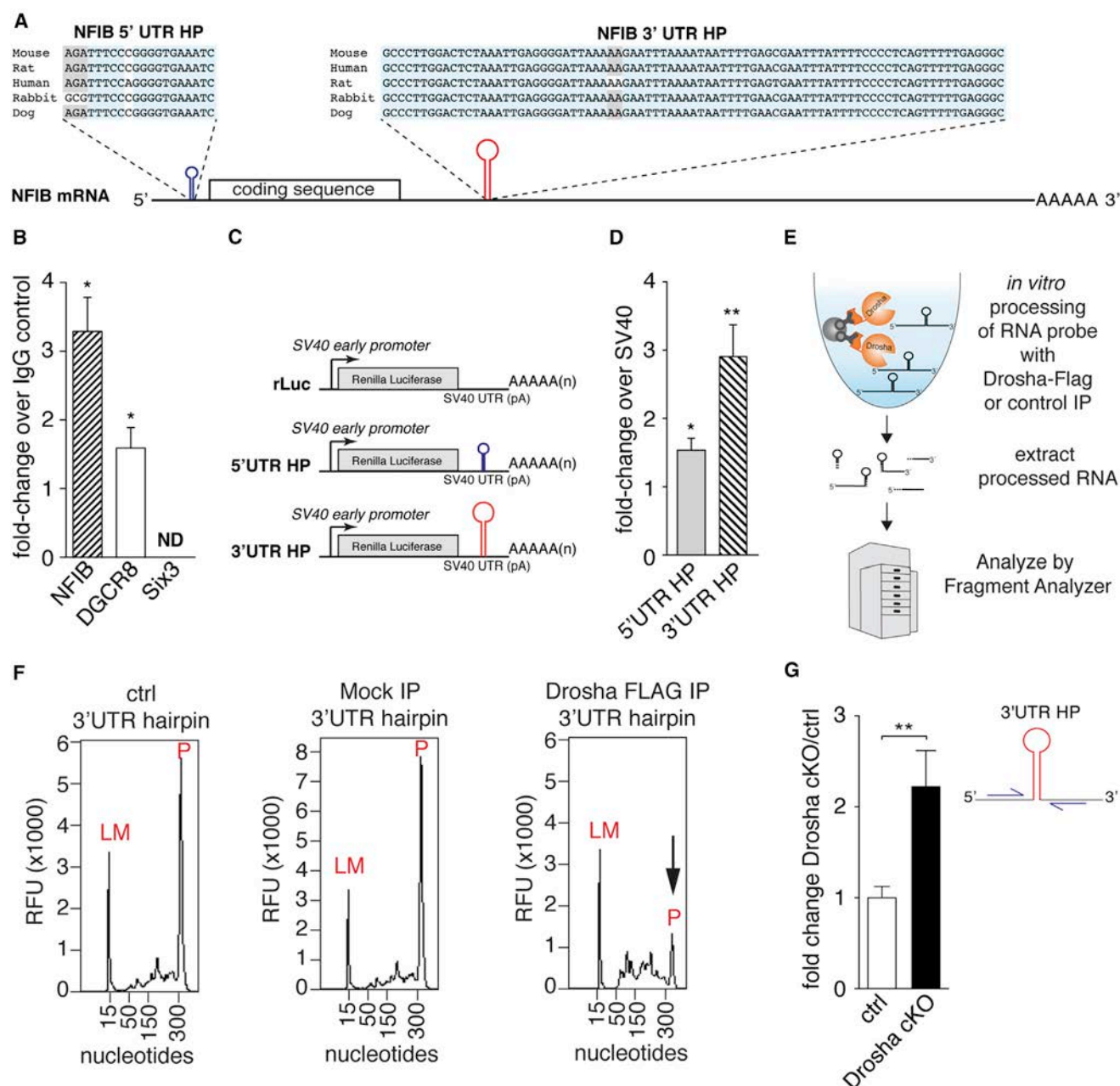


Figure 3. Drosha Binds and Cleaves NFIB mRNA in DG NSCs

(A) Evolutionary conserved hairpins 5' UTR HP (blue) and 3' UTR HP (red) in the NFIB mRNA sequence.

(B) Drosha CLIP-qRT-PCR of NFIB mRNA from DG NSCs. DGCR8 and Six3 mRNAs were used as positive and negative control CLIP targets, respectively (n = 3 replicates). Mann-Whitney test: *p < 0.05.

(C) Scheme of the psiCheck Renilla Luciferase constructs (rLuc) containing the NFIB 5' UTR HP or 3' UTR HP sequence in the SV40 UTR.

(D) qRT-PCR analysis of rLuc mRNA pulled down with Drosha from psiCheck-NFIB 5' UTR HP and psiCheck-NFIB 3' UTR HP transfected N2a cells relative to the pull-down from psiCheck-rLuc transfected cells (n = 3 replicates). Two-sided Student's t test: *p < 0.05, **p < 0.01.

(E) Scheme of the in vitro processing procedure.

(F) Capillary electrophoresis electropherograms of NFIB 3' UTR HP RNA (probe) incubated with the beads alone (ctrl), incubated with mock IP sample, or flag-tagged Drosha IP (Drosha FLAG IP). Arrow points to degraded 3' UTR HP probe. Loading marker (LM) and probe (P) are indicated.

(G) qRT-PCR analysis of the NFIB 3' UTR HP in control and Drosha cKO NSCs 2 days after adeno-Cre infection.

Data are mean ± SEM.

regulation to NSC maintenance and differentiation. Growing evidence suggest that miRNA-independent functions of the microprocessor are conserved mechanisms that regulate several

cellular processes in the nervous system and other tissues (Chong et al., 2010; Han et al., 2009; Karginov et al., 2010; Knuckles et al., 2012; Macias et al., 2012).

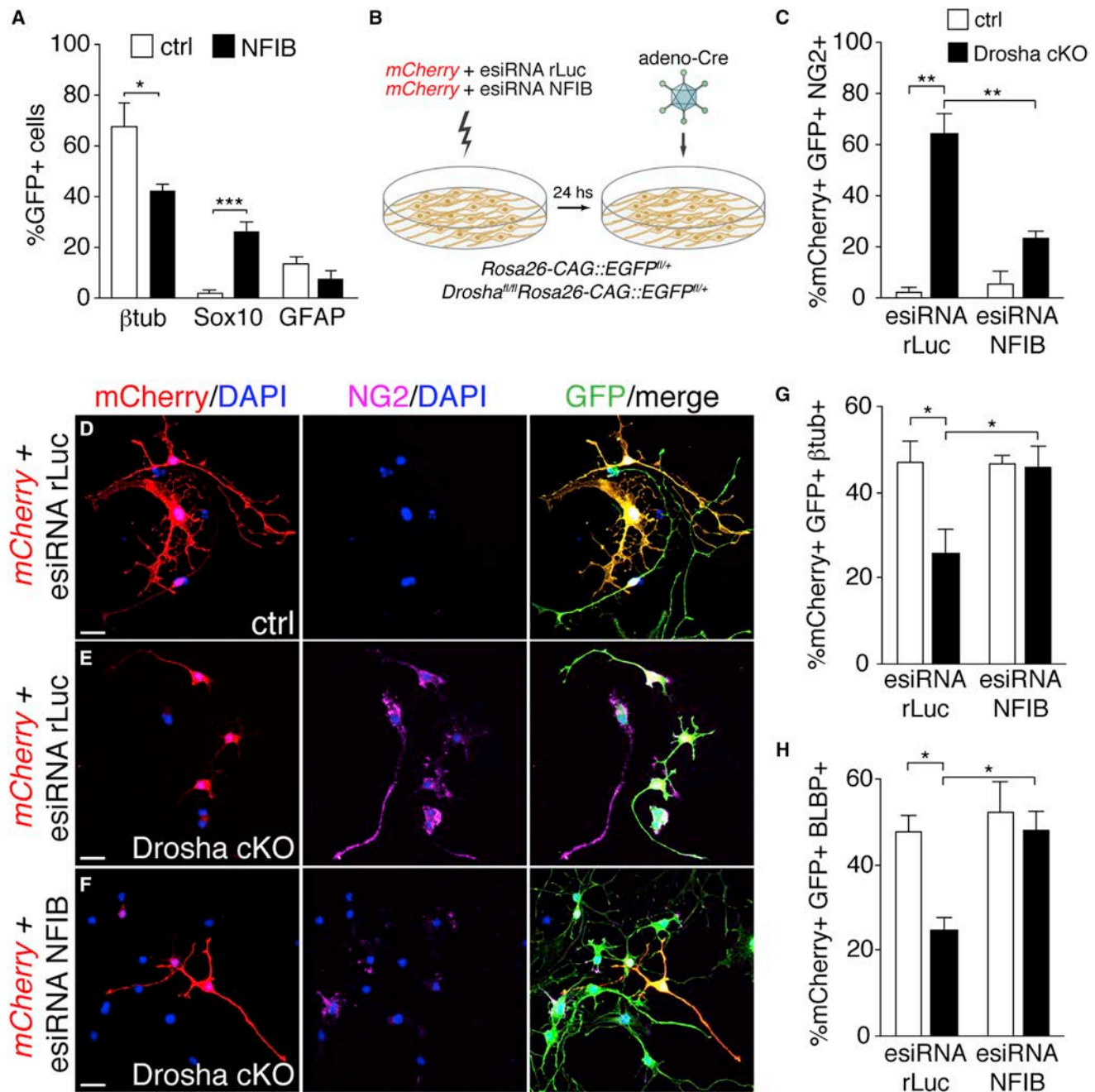


Figure 4. NFIB Knockdown Rescues Drosha cKO-Induced Oligodendrocyte Differentiation

(A) Quantification of lineage marker expression by NFIB overexpressing DG NSCs after 5-days of differentiation (n = 3 replicates). Mann-Whitney test: *p < 0.05, ***p < 0.001.

(B) Experimental paradigm of the nucleofection experiments.

(C) Quantification of adeno-Cre virus infected (GFP⁺) mCherry⁺NG2⁺ OPCs in Drosha cKO and control NSCs nucleofected with control rLuc esiRNA or NFIB esiRNA.

(D–F) mCherry⁺, GFP⁺, and NG2⁺ cells in adeno-Cre virus infected control NSC cultures nucleofected with the control esiRNA (D), Drosha cKO NSCs nucleofected with the control esiRNA (E), and Drosha cKO NSCs nucleofected with the NFIB esiRNA (F).

(G) Quantification of adeno-Cre virus infected (GFP⁺) mCherry⁺ β tub⁺ neurons from Drosha cKO and control NSCs nucleofected with rLuc esiRNA or NFIB esiRNA.

(H) Quantification of adeno-Cre virus infected (GFP⁺) mCherry⁺BLBP⁺ progenitors from Drosha cKO and control NSCs nucleofected with control rLuc esiRNA or NFIB esiRNA.

Data are mean \pm SEM. Biological replicates, n = 3. Kruskal-Wallis with Dunn post hoc test: *p < 0.05, **p < 0.01. The scale bars represent 20 μ m.

Here we show that Drosha plays a central role in regulating progenitors of the adult DG by sustaining NSC potential. Upon *Drosha* ablation, DG NSCs are depleted, and gliogenesis increases at the expense of neurogenesis. By comparing *Drosha* cKO and *Dicer* cKO mice, we identified the transcription factor NFIB as a target of Drosha and showed that the blockade of NFIB expression is necessary for inhibiting oligodendrocyte formation and enabling neurogenesis in the adult DG. Therefore, Drosha regulates DG neurogenesis and gliogenesis at least partially through a miRNA and *Dicer*-independent, cell-intrinsic fate program.

CLIP experiments revealed that the microprocessor targets different RNA classes, including pri-miRNAs, small nucleolar RNA, long non-coding RNA, and mRNAs (Macias et al., 2012). The microprocessor interactome has been defined in human embryonic stem cells and indicates the importance of cell type and biological context (Seong et al., 2014). However, it is clear that several mRNAs are processed by the microprocessor, resulting in their destabilization (Chong et al., 2010; Johanson et al., 2015; Knuckles et al., 2012). The non-canonical functions of the microprocessor represent a rapid and efficient way to influence gene expression. Our understanding of the mechanisms underlying these alternative functions of Drosha and the microprocessor need further investigation. The Drosha-DGCR8 complex is required for miRNA biogenesis, but it is possible that other protein-protein interactions underlie the alternate functions of Drosha (Macias et al., 2015).

DG NSCs are fate committed to glutamatergic granule neuron and astrocytic fates in vivo (Bonaguidi et al., 2011; Lugert et al., 2010). How this intrinsic fate restriction is controlled remained unclear. In vitro studies showed that DG NSCs are able to generate oligodendrocytes only under specific conditions, including co-culture with neurons (Song et al., 2002; Suh et al., 2007). Furthermore, reprogramming of adult DG NSCs by *Ascl1* overexpression leads to a shift in fate from neuronal to oligodendrocyte differentiation (Braun et al., 2015; Jessberger et al., 2008). A potential link between Drosha and *Ascl1* remains to be shown, but *Ascl1* mRNA was not cross-linked immunoprecipitated with Drosha from DG NSCs (data not shown).

Clonal lineage tracing of DG NSCs in vivo showed symmetric and asymmetric neuron and astrocytic fates (Bonaguidi et al., 2011). *Drosha* cKO NSCs exited the stem cell pool and the cell cycle and generated few progeny. However, at the population and single-cell levels, DG NSCs retain the potential to generate all three cell lineages of the brain, but Drosha mediates the intrinsic restriction of oligodendrocyte differentiation potential.

NFI transcription factors can activate and repress gene transcription depending on the gene and cellular context (Chang et al., 2013; Gronostajski, 2000; Messina et al., 2010). NFIB influences stem cell maintenance and differentiation in several tissues, including in the SVZ, as part of a cross-regulatory network together with Pax6/Brg1 (Chang et al., 2013; Ninkovic et al., 2013). In addition, NFIB can repress Notch signaling in embryonic hippocampal NSCs by repressing *Hes1* promoter activity (Piper et al., 2010). Therefore, we speculate that induction of NFIB expression might lead to inhibition of stem cell genes and block of Notch signaling resulting in exhaustion of the DG NSC pool and differentiation. Moreover, we also show for the first

time that NFIB has a central function in regulating oligodendrocyte fate commitment in the adult DG. It remains to be shown which genes are regulated downstream of NFIB. Although we cannot exclude that NFIB acts as a transcriptional repressor of genes required for neuronal differentiation and therefore indirectly promotes gliogenesis, NG2 is upregulated in response to *Drosha* cKO in an NFIB-dependent manner. Interestingly, *Cspg4* (the gene encoding NG2) has NFI binding motifs that are bound by NFIB, suggesting a direct regulation in DG NSCs (Chang et al., 2013). We believe this is the first demonstration of a non-canonical Drosha-mediated regulation of adult stem cell fate through a niche-independent intrinsic pathway. In the future, it will be important to understand the targets of this post-transcriptional pathway and whether stem cells are able to modulate Drosha activity to control cell fate in order to satisfy demand.

EXPERIMENTAL PROCEDURES

Animal Husbandry

The mice used have been described previously (Supplemental Experimental Procedures). Mice were maintained on a 12 hr day-night cycle with free access to food and water under specific pathogen-free conditions and according to Swiss federal regulations. All procedures were approved by the Basel Cantonal Veterinary Office (license numbers 2537 and 2538).

Hippocampal NSC Cultures, Adenoviral Infection, and Nucleofection

DG NSCs were isolated from 8-week-old mice as described previously (Lugert et al., 2010). DG NSCs were infected with an adeno-Cre adenovirus at a multiplicity of infection of 100 and fixed after 24 or 48 hr. DG NSC cultures were nucleofected using a mouse neural stem cell kit (Lonza) (Supplemental Experimental Procedures).

FACS

After TAM induction, NSCs were isolated from *Hes5CreER^{T2}Rosa26-CAG::EGFP^{fl/+}* and *Hes5::CreER^{T2}Drosha^{fl/fl}Rosa26-CAG::EGFP^{fl/+}* using a FACSAriaIII (BD Biosciences) (Supplemental Experimental Procedures).

RNA Isolation, qRT-PCR, and Analysis of miRNA Expression

Total RNA was isolated from cultured or sorted DG NSCs using Trizol reagent (Life Technologies). Analysis of gene expression was performed as described in Supplemental Experimental Procedures. miRNAs were isolated using mirVANA kit (ThermoFisher) following the miRNA enrichment procedure and quantified by TaqMan arrays (Life Technologies) (Supplemental Experimental Procedures).

In Vitro Processing of NFIB HP RNAs

In vitro processing was performed on 5' and 3' UTR NFIB HP RNAs as described previously with minor adaptations (Supplemental Experimental Procedures) (Lee and Kim, 2007).

5' RACE

5' RACE experiments were performed on 3 μ g of total RNA of control and *Drosha* cKO NSCs following the manufacturer's instructions (Invitrogen) (Supplemental Experimental Procedures).

Luciferase Assay

DG NSCs were transduced with an adeno-Cre adenovirus at a multiplicity of infection of 100 with or without subsequent nucleofection 2 days later with the psiCheck2 containing the 3' UTR HP or 5' UTR HP or control psiCheck2 vectors (Supplemental Experimental Procedures).

Quantification and Statistical Analysis

Randomly selected, stained cells were analyzed with fixed photomultiplier settings on a Zeiss LSM510 confocal and Apotome2 microscope. For clonal

analysis, the entire hippocampus was sectioned and reconstructed as described previously (Bonaguidi et al., 2011) (Supplemental Experimental Procedures). Percentages were converted by arcsine transformation. Statistical comparisons were conducted by two-tailed unpaired Student's *t* test, Mann-Whitney test, one-way ANOVA, or Kruskal-Wallis with Dunn post hoc test as indicated. Statistical significance was assessed using GraphPad Prism software (GraphPad Software). Significance was established at *p* < 0.05.

SUPPLEMENTAL INFORMATION

Supplemental Information includes Supplemental Experimental Procedures, four figures, and four tables and can be found with this article online at <http://dx.doi.org/10.1016/j.stem.2016.07.003>.

AUTHOR CONTRIBUTIONS

C.R., A. Erni, A.G., R.B., A. Engler, P.J.G., and M.M. designed and performed experiments and evaluated and interpreted the data. T.W. and S.J. contributed reagents. V.T. conceived and designed the project and evaluated the data. C.R., A. Erni, and V.T. wrote the paper and prepared the figures. All authors edited and proofread the manuscript.

ACKNOWLEDGMENTS

We thank Dr. H. Song and the members of the V.T. laboratory for helpful discussions and Frank Sager for excellent technical assistance. We thank Drs. A. Alvarez-Buylla, K. Obernier, D. Littmann, M. Chong, and H. Schrewe for providing reagents. We thank the BioOptics Facility of the Department of Biomedicine and the Animal Core Facility of the University of Basel. T.W. was supported by a Boehringer Ingelheim Fonds fellowship. This work was supported by the Swiss National Science Foundation (310030_143767).

Received: August 3, 2015

Revised: May 23, 2016

Accepted: July 6, 2016

Published: August 18, 2016

REFERENCES

- Barry, G., Piper, M., Lindwall, C., Moldrich, R., Mason, S., Little, E., Sarkar, A., Tole, S., Gronostajski, R.M., and Richards, L.J. (2008). Specific glial populations regulate hippocampal morphogenesis. *J. Neurosci.* 28, 12328–12340.
- Bonaguidi, M.A., Wheeler, M.A., Shapiro, J.S., Stadel, R.P., Sun, G.J., Ming, G.L., and Song, H. (2011). In vivo clonal analysis reveals self-renewing and multipotent adult neural stem cell characteristics. *Cell* 145, 1142–1155.
- Braun, S.M., Pilz, G.A., Machado, R.A., Moss, J., Becher, B., Toni, N., and Jessberger, S. (2015). Programming Hippocampal Neural Stem/Progenitor Cells into Oligodendrocytes Enhances Remyelination in the Adult Brain after Injury. *Cell Rep.* 11, 1679–1685.
- Chang, C.Y., Pasolli, H.A., Giannopoulou, E.G., Guasch, G., Gronostajski, R.M., Elemento, O., and Fuchs, E. (2013). NFIB is a governor of epithelial-melanocyte stem cell behaviour in a shared niche. *Nature* 495, 98–102.
- Chong, M.M., Zhang, G., Cheloufi, S., Neubert, T.A., Hannon, G.J., and Littman, D.R. (2010). Canonical and alternate functions of the microRNA biogenesis machinery. *Genes Dev.* 24, 1951–1960.
- Davis, T.H., Cuellar, T.L., Koch, S.M., Barker, A.J., Harfe, B.D., McManus, M.T., and Ullian, E.M. (2008). Conditional loss of Dicer disrupts cellular and tissue morphogenesis in the cortex and hippocampus. *J. Neurosci.* 28, 4322–4330.
- Deneen, B., Ho, R., Lukaszewicz, A., Hochstim, C.J., Gronostajski, R.M., and Anderson, D.J. (2006). The transcription factor NFIA controls the onset of gliogenesis in the developing spinal cord. *Neuron* 52, 953–968.
- Encinas, J.M., Michurina, T.V., Peunova, N., Park, J.H., Tordo, J., Peterson, D.A., Fishell, G., Koulakov, A., and Enikolopov, G. (2011). Division-coupled astrocytic differentiation and age-related depletion of neural stem cells in the adult hippocampus. *Cell Stem Cell* 8, 566–579.
- Gronostajski, R.M. (2000). Roles of the NF1/CTF gene family in transcription and development. *Gene* 249, 31–45.
- Ha, M., and Kim, V.N. (2014). Regulation of microRNA biogenesis. *Nat. Rev. Mol. Cell Biol.* 15, 509–524.
- Hack, M.A., Sugimori, M., Lundberg, C., Nakafuku, M., and Götz, M. (2004). Regionalization and fate specification in neurospheres: the role of Olig2 and Pax6. *Mol. Cell. Neurosci.* 25, 664–678.
- Han, J., Pedersen, J.S., Kwon, S.C., Belair, C.D., Kim, Y.K., Yeom, K.H., Yang, W.Y., Haussler, D., Belloch, R., and Kim, V.N. (2009). Posttranscriptional crossregulation between Drosha and DGCR8. *Cell* 136, 75–84.
- Harris, L., Genovesi, L.A., Gronostajski, R.M., Wainwright, B.J., and Piper, M. (2015). Nuclear factor one transcription factors: Divergent functions in developmental versus adult stem cell populations. *Dev. Dyn.* 244, 227–238.
- Hüttmann, K., Sadgrove, M., Wallraff, A., Hinterkeuser, S., Kirchhoff, F., Steinhäuser, C., and Gray, W.P. (2003). Seizures preferentially stimulate proliferation of radial glia-like astrocytes in the adult dentate gyrus: functional and immunocytochemical analysis. *Eur. J. Neurosci.* 18, 2769–2778.
- Ihrle, R.A., and Alvarez-Buylla, A. (2011). Lake-front property: a unique germinal niche by the lateral ventricles of the adult brain. *Neuron* 70, 674–686.
- Jessberger, S., Toni, N., Clemenson, G.D., Jr., Ray, J., and Gage, F.H. (2008). Directed differentiation of hippocampal stem/progenitor cells in the adult brain. *Nat. Neurosci.* 11, 888–893.
- Johanson, T.M., Keown, A.A., Cmero, M., Yeo, J.H., Kumar, A., Lew, A.M., Zhan, Y., and Chong, M.M. (2015). Drosha controls dendritic cell development by cleaving messenger RNAs encoding inhibitors of myelopoiesis. *Nat. Immunol.* 16, 1134–1141.
- Kang, P., Lee, H.K., Glasgow, S.M., Finley, M., Danti, T., Gaber, Z.B., Graham, B.H., Foster, A.E., Novitsch, B.G., Gronostajski, R.M., and Deneen, B. (2012). Sox9 and NFIA coordinate a transcriptional regulatory cascade during the initiation of gliogenesis. *Neuron* 74, 79–94.
- Karginov, F.V., Cheloufi, S., Chong, M.M., Stark, A., Smith, A.D., and Hannon, G.J. (2010). Diverse endonucleolytic cleavage sites in the mammalian transcriptome depend upon microRNAs, Drosha, and additional nucleases. *Mol. Cell* 38, 781–788.
- Knuckles, P., Vogt, M.A., Lugert, S., Milo, M., Chong, M.M., Hautbergue, G.M., Wilson, S.A., Littman, D.R., and Taylor, V. (2012). Drosha regulates neurogenesis by controlling neurogenin 2 expression independent of microRNAs. *Nat. Neurosci.* 15, 962–969.
- Kriegstein, A., and Alvarez-Buylla, A. (2009). The glial nature of embryonic and adult neural stem cells. *Annu. Rev. Neurosci.* 32, 149–184.
- Kronenberg, G., Reuter, K., Steiner, B., Brandt, M.D., Jessberger, S., Yamaguchi, M., and Kempermann, G. (2003). Subpopulations of proliferating cells of the adult hippocampus respond differently to physiologic neurogenic stimuli. *J. Comp. Neurol.* 467, 455–463.
- Lee, Y., and Kim, V.N. (2007). In vitro and in vivo assays for the activity of Drosha complex. In *Methods in Enzymology* (Academic Press), pp. 87–106.
- Lugert, S., Basak, O., Knuckles, P., Haussler, U., Fabel, K., Götz, M., Haas, C.A., Kempermann, G., Taylor, V., and Giachino, C. (2010). Quiescent and active hippocampal neural stem cells with distinct morphologies respond selectively to physiological and pathological stimuli and aging. *Cell Stem Cell* 6, 445–456.
- Lugert, S., Vogt, M., Tchorz, J.S., Müller, M., Giachino, C., and Taylor, V. (2012). Homeostatic neurogenesis in the adult hippocampus does not involve amplification of Ascl1(high) intermediate progenitors. *Nat. Commun.* 3, 670.
- Macias, S., Plass, M., Stajuda, A., Michlewski, G., Eyra, E., and Cáceres, J.F. (2012). DGCR8 HITS-CLIP reveals novel functions for the Microprocessor. *Nat. Struct. Mol. Biol.* 19, 760–766.
- Macias, S., Cordiner, R.A., Gautier, P., Plass, M., and Cáceres, J.F. (2015). DGCR8 acts as an adaptor for the exosome complex to degrade double-stranded structured RNAs. *Mol. Cell* 60, 873–885.
- Menn, B., Garcia-Verdugo, J.M., Yaschine, C., Gonzalez-Perez, O., Rowitch, D., and Alvarez-Buylla, A. (2006). Origin of oligodendrocytes in the subventricular zone of the adult brain. *J. Neurosci.* 26, 7907–7918.

- Merkle, F.T., Mirzadeh, Z., and Alvarez-Buylla, A. (2007). Mosaic organization of neural stem cells in the adult brain. *Science* 317, 381–384.
- Messina, G., Biressi, S., Monteverde, S., Magli, A., Cassano, M., Perani, L., Roncaglia, E., Tagliafico, E., Starnes, L., Campbell, C.E., et al. (2010). Nfix regulates fetal-specific transcription in developing skeletal muscle. *Cell* 140, 554–566.
- Ninkovic, J., Steiner-Mezzadri, A., Jawerka, M., Akinci, U., Masserdotti, G., Petricca, S., Fischer, J., von Holst, A., Beckers, J., Lie, C.D., et al. (2013). The BAF complex interacts with Pax6 in adult neural progenitors to establish a neurogenic cross-regulatory transcriptional network. *Cell Stem Cell* 13, 403–418.
- Pedersen, J.S., Bejerano, G., Siepel, A., Rosenbloom, K., Lindblad-Toh, K., Lander, E.S., Kent, J., Miller, W., and Haussler, D. (2006). Identification and classification of conserved RNA secondary structures in the human genome. *PLoS Comput. Biol.* 2, e33.
- Petrus, D.S., Fabel, K., Kronenberg, G., Winter, C., Steiner, B., and Kempermann, G. (2009). NMDA and benzodiazepine receptors have synergistic and antagonistic effects on precursor cells in adult hippocampal neurogenesis. *Eur. J. Neurosci.* 29, 244–252.
- Piper, M., Barry, G., Hawkins, J., Mason, S., Lindwall, C., Little, E., Sarkar, A., Smith, A.G., Moldrich, R.X., Boyle, G.M., et al. (2010). NFIA controls telencephalic progenitor cell differentiation through repression of the Notch effector Hes1. *J. Neurosci.* 30, 9127–9139.
- Santarelli, L., Saxe, M., Gross, C., Surget, A., Battaglia, F., Dulawa, S., Weisstaub, N., Lee, J., Duman, R., Arancio, O., et al. (2003). Requirement of hippocampal neurogenesis for the behavioral effects of antidepressants. *Science* 301, 805–809.
- Seong, Y., Lim, D.H., Kim, A., Seo, J.H., Lee, Y.S., Song, H., and Kwon, Y.S. (2014). Global identification of target recognition and cleavage by the Microprocessor in human ES cells. *Nucleic Acids Res.* 42, 12806–12821.
- Sierra, A., Martín-Suárez, S., Valcárcel-Martín, R., Pascual-Brazo, J., Aelvoet, S.A., Abiega, O., Deudero, J.J., Brewster, A.L., Bernales, I., Anderson, A.E., et al. (2015). Neuronal hyperactivity accelerates depletion of neural stem cells and impairs hippocampal neurogenesis. *Cell Stem Cell* 16, 488–503.
- Song, H., Stevens, C.F., and Gage, F.H. (2002). Astroglia induce neurogenesis from adult neural stem cells. *Nature* 417, 39–44.
- Steele-Perkins, G., Plachez, C., Butz, K.G., Yang, G., Bachurski, C.J., Kinsman, S.L., Litwack, E.D., Richards, L.J., and Gronostajski, R.M. (2005). The transcription factor gene Nfib is essential for both lung maturation and brain development. *Mol. Cell. Biol.* 25, 685–698.
- Steiner, B., Zurborg, S., Hörster, H., Fabel, K., and Kempermann, G. (2008). Differential 24 h responsiveness of Prox1-expressing precursor cells in adult hippocampal neurogenesis to physical activity, environmental enrichment, and kainic acid-induced seizures. *Neuroscience* 154, 521–529.
- Suh, H., Consiglio, A., Ray, J., Sawai, T., D’Amour, K.A., and Gage, F.H. (2007). In vivo fate analysis reveals the multipotent and self-renewal capacities of Sox2+ neural stem cells in the adult hippocampus. *Cell Stem Cell* 1, 515–528.
- Sun, G.J., Zhou, Y., Ito, S., Bonaguidi, M.A., Stein-O’Brien, G., Kawasaki, N.K., Modak, N., Zhu, Y., Ming, G.L., and Song, H. (2015). Latent tri-lineage potential of adult hippocampal neural stem cells revealed by Nf1 inactivation. *Nat. Neurosci.* 18, 1722–1724.

Cell Stem Cell, Volume 19

Supplemental Information

Multipotency of Adult Hippocampal NSCs In Vivo

Is Restricted by Drosha/NFIB

Chiara Rolando, Andrea Erni, Alice Grison, Robert Beattie, Anna Engler, Paul J. Gokhale, Marta Milo, Thomas Wegleiter, Sebastian Jessberger, and Verdon Taylor

Figure S1, Related to Figure 1

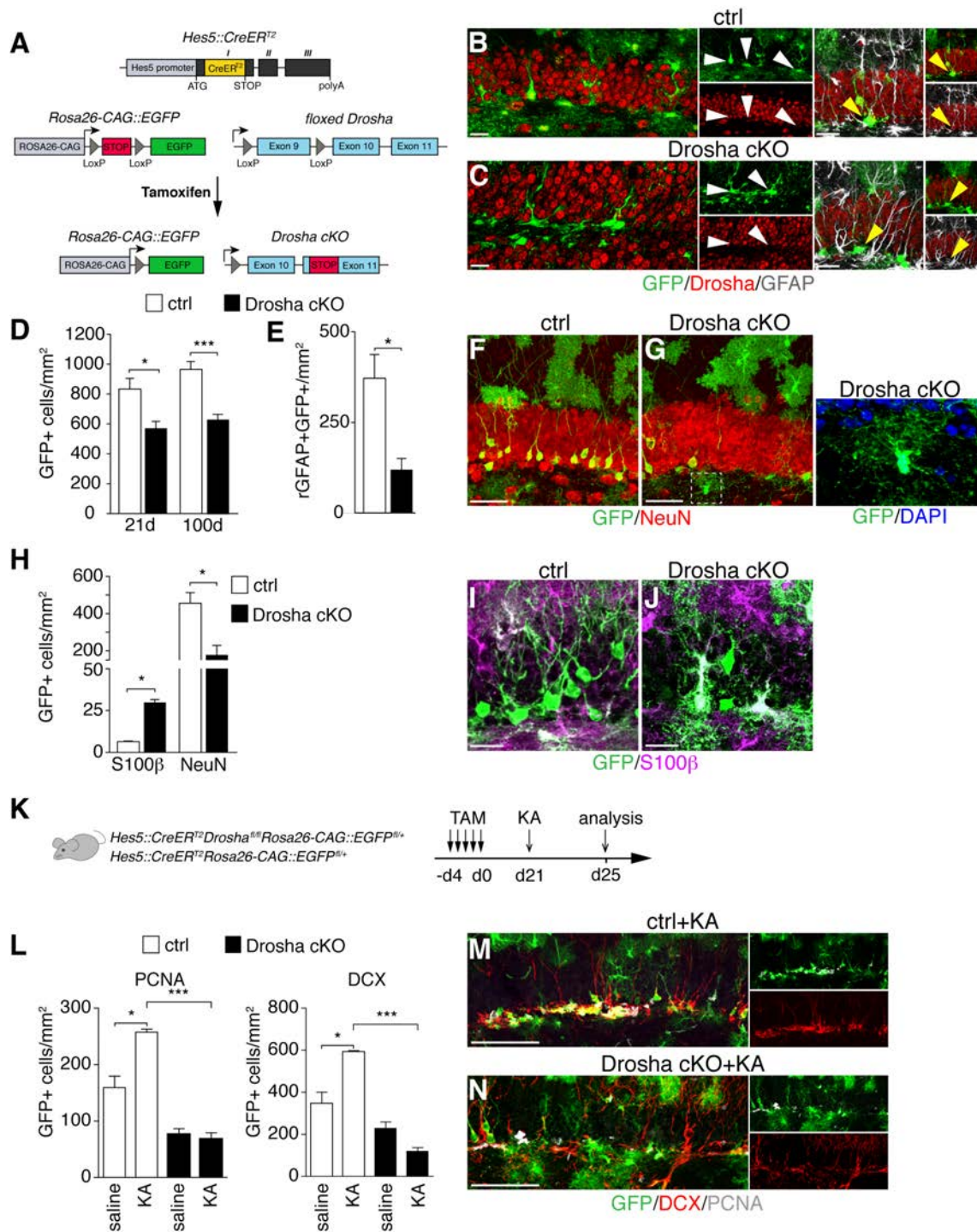


Figure S1. Drosha cKO from *Hes5::CreER^{T2}* expressing NSCs impairs neurogenesis in the DG. (A) Overview of the *Hes5::CreER^{T2}*, *Rosa26-CAG::EGFP* and floxed *Drosha* alleles and Cre-mediated gene rearrangements (Chong et al., 2008; Harfe et al., 2005; Lugert et al., 2012). TAM treatment induces Drosha cKO and constitutive expression of GFP from the *Rosa26-CAG::EGFP* reporter allele in *Hes5::CreER^{T2}*-expressing cells and their progeny. (B) Twenty-one days after TAM induction, GFP⁺ *Hes5*-derived cells in control animals express Drosha (white arrowheads) and these include radial GFP⁺GFAP⁺ NSCs (yellow arrowheads). (C) Twenty-one days after TAM induction, GFP⁺ *Hes5*-derived cells do not express Drosha in the Drosha cKO (white arrowheads) including *Hes5*-derived radial GFP⁺GFAP⁺ (yellow arrowheads). (D) Quantification of *Hes5*-derived (GFP⁺) cells at d21 and d100 post-TAM induction in control and Drosha cKO animals (control *n* = 5, Drosha cKO *n* = 5. Two-sided

Student's t-test, $*P<0.05$, $***P<0.001$). (E) Quantification of radial GFP⁺GFAP⁺ cells at d21 post-TAM induction in control and Drosha cKO animals (control $n = 5$, Drosha cKO $n = 5$. Two-sided Student's t-test, $*P<0.05$). (F and G) NeuN⁺ mature neurons in control and Drosha cKO animals at d100 post-TAM induction. Inset and magnification on the right show an oligodendrocyte in Drosha cKO animals at d100 post-TAM induction. (H) Quantification of GFP⁺S100 β ⁺ astrocytes and GFP⁺NeuN⁺ newborn neurons at d100 post-TAM induction in control and Drosha cKO animals (control $n = 5$, Drosha cKO $n = 5$. Two-sided Student's t-test, $*P<0.05$). (I and J) S100 β ⁺ mature astrocytes in the Drosha cKO compared to control animals at d100. (K) TAM induction and kainic acid (KA) treatment regime to study the activation of Drosha cKO progenitors after epileptic seizures. TAM was administered once per day for 5 consecutive days. KA was administered systemically 21 days after TAM induction and the mice analyzed 4 days later at d25. (L) Quantification of proliferative GFP⁺PCNA⁺ progenitors and GFP⁺DCX⁺ neuroblasts on d4 after KA treatment in control and Drosha cKO animals. (M and N) PCNA⁺ and DCX⁺ cells in control and Drosha cKO animals on d4 after KA treatment (control $n = 3$, Drosha cKO $n = 4$. One-way ANOVA with Bonferroni post-hoc test: $*P<0.05$, $***P<0.001$). Data are mean \pm SEM. Scale bars represent 20 μ m in (B), (C), (F), (G), (I) and (J) and represent 100 μ m in (M) and (N).

Figure S2, Related to Figure 2

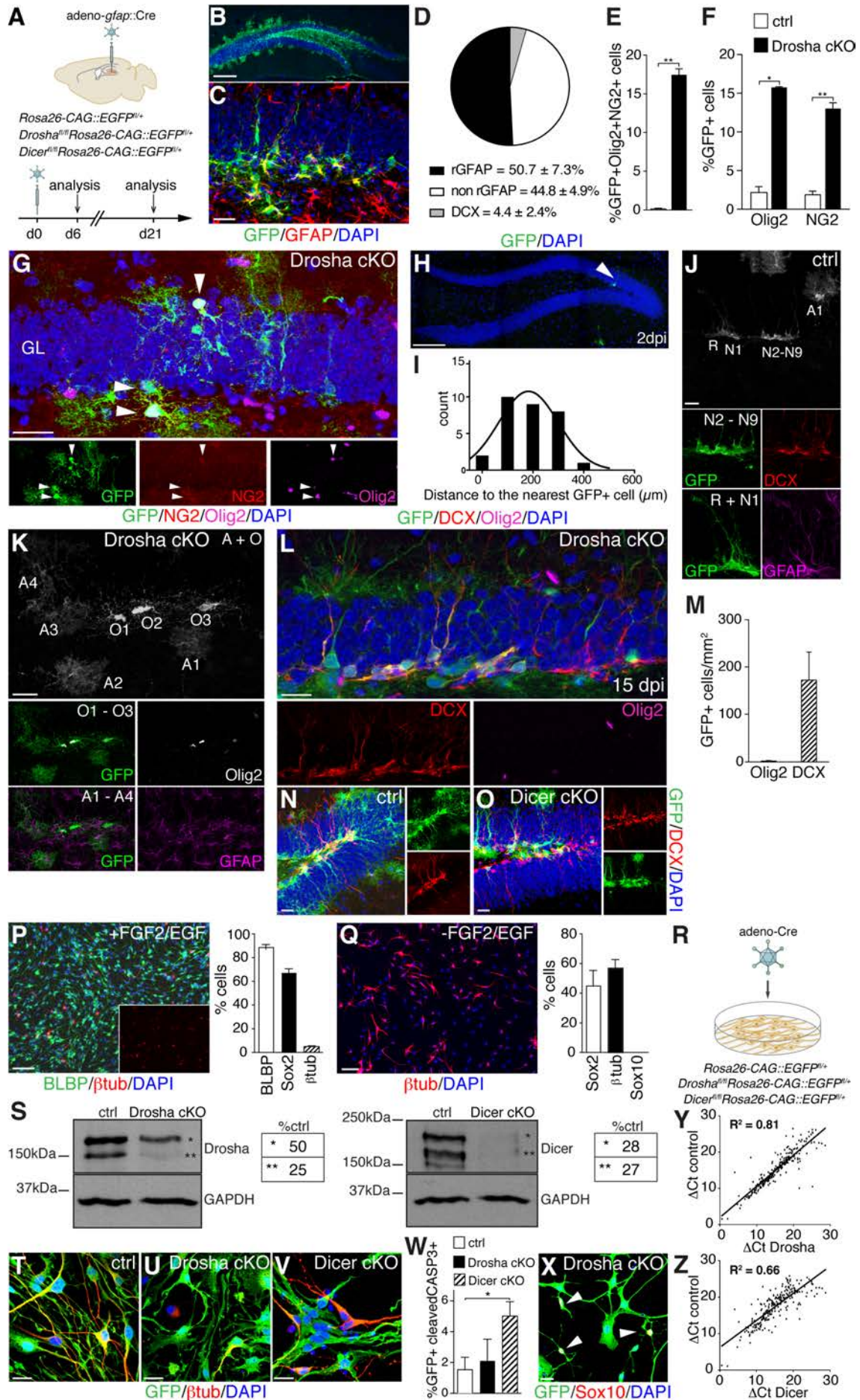


Figure S2. Adult hippocampal NSCs produce oligodendrocytes upon Droscha deletion *in vivo* and *in vitro*. (A) Experimental paradigm of adeno-*gfap::Cre* stereotactic intracranial injection and gene deletion from GFAP⁺ radial NSCs and analysis at d6 and d21. (B) GFP expression from the recombined *Rosa26-CAG::EGFP*^{f/+} allele following adeno-*gfap::Cre* injection into the DG of *Rosa26-CAG::EGFP*^{f/+} mice. (C) GFP and GFAP expression at 6 dpi. (D) Quantification of GFP⁺GFAP⁺ and GFP⁺DCX⁺ at 6 dpi. (E) Quantification of GFP⁺Olig2⁺NG2⁺ cells in the DG of Droscha cKO (*Hes5::CreER^{T2}Droscha^{f/f}Rosa26-CAG::EGFP^{f/+}*) and control (*Hes5::CreER^{T2}Rosa26-CAG::EGFP^{f/+}*) animals (control *n* = 3, Droscha cKO *n* = 3. Two-sided Student's t-test: ***P*<0.01). (F) Quantification of GFP⁺Olig2⁺ and GFP⁺NG2⁺ cells in Droscha cKO (*Hes5::CreER^{T2}Droscha^{f/f}Rosa26-CAG::EGFP^{f/+}*) DG NSCs and control (*Hes5::CreER^{T2}Rosa26-CAG::EGFP^{f/+}*) animals (control *n* = 3, Droscha cKO *n* = 3. Two-sided Student's t-test: **P*<0.05, ***P*<0.01). (G) NG2⁺ and Olig2⁺ oligodendrocytes in the DG of Droscha cKO (*Hes5::CreER^{T2}Droscha^{f/f}Rosa26-CAG::EGFP^{f/+}*) at d21 post-TAM induction (arrowheads). (H) Clonal analysis of GFP expression following low dose TAM administration of *Hes5::CreER^{T2}Rosa26-CAG::EGFP^{f/+}* mice after 2 days. (I) Quantification of the distance to the nearest GFP⁺ cell 2 days after low dose TAM induction (*n* = 2 animals). (J) GFP, DCX and GFAP expression following low dose TAM administration of *Hes5::CreER^{T2}Rosa26-CAG::EGFP^{f/+}* animals after 21 days. A - astrocyte, N - neuron, R - radial glia. The cells of each cell-type in the clone are numbered in the image. (K) GFP, Olig2 and GFAP expression following low dose TAM induction of Droscha cKO at d21. A - astrocyte and O - oligodendrocyte. The cells of each cell-type in the clone are numbered in the image. (L) GFP, DCX and Olig2 expression d15 after retro-Cre virus infection of the DG of *Droscha^{f/f}Rosa26-CAG::EGFP^{f/+}* animals. (M) Quantification of GFP⁺DCX and GFP⁺Olig2 cells d15 after retro-Cre virus infection of the DG of *Droscha^{f/f}Rosa26-CAG::EGFP^{f/+}* animals. (N and O) GFP and DCX expression after adeno-*gfap::Cre*-mediated Dicer cKO (*Hes5::CreER^{T2}Dicer^{f/f}Rosa26-CAG::EGFP^{f/+}*) and infected control (*Hes5::CreER^{T2}Rosa26-CAG::EGFP^{f/+}*) mice. (P) Expression and quantification of BLBP⁺ and β tub⁺ cells derived from NSCs grown in the presence of mitogens (FGF2 and EGF). (Q) β tub expression by cultured DG NSCs upon differentiation induced by mitogen removal and quantification of Sox2, β tub and Sox10 expressing cells (Biological replicates *n* = 2). (R) Experimental paradigm for gene ablation from cultured adult DG NSCs with adeno-Cre viruses. (S) Western-blot and quantification of Droscha and Dicer protein expression 72 hours after adeno-Cre virus mediated Droscha cKO and Dicer cKO, respectively. (T-V) β tub expression after adeno-Cre virus mediated Droscha cKO and Dicer cKO compared to control. (W) Quantification of GFP⁺cleavedCASP3⁺ cells in cultured control, Droscha cKO and Dicer cKO NSCs d4 post adeno-Cre virus infection (Biological replicates *n* = 4. Kruskal-Wallis with Dunn post-hoc test: **P*<0.05). (X) Cells expressing the oligodendrocyte marker Sox10 by Droscha cKO cells 2 days after adeno-Cre virus infection. (Y) Δ CT plots of relative miRNA expression profiles of control (y-axis) versus Droscha cKO (x-axis) DG NSC cultures 48 hours post adeno-Cre infection. Correlation coefficients R^2 = 0.81. (Z) Δ CT plots of relative miRNA expression profiles of control (y-axis) versus Dicer cKO (x-axis) DG NSC cultures 48 hours post adeno-Cre infection. Correlation coefficients R^2 = 0.66. Data are mean \pm SEM. Scale bars represent 200 μ m in (B), 100 μ m in (H), (P) and (Q), 20 μ m in (C), (G), (J), (K), (L), (N), (O), (T), (U), (V) and (X).

Figure S3, Related to Figure 3

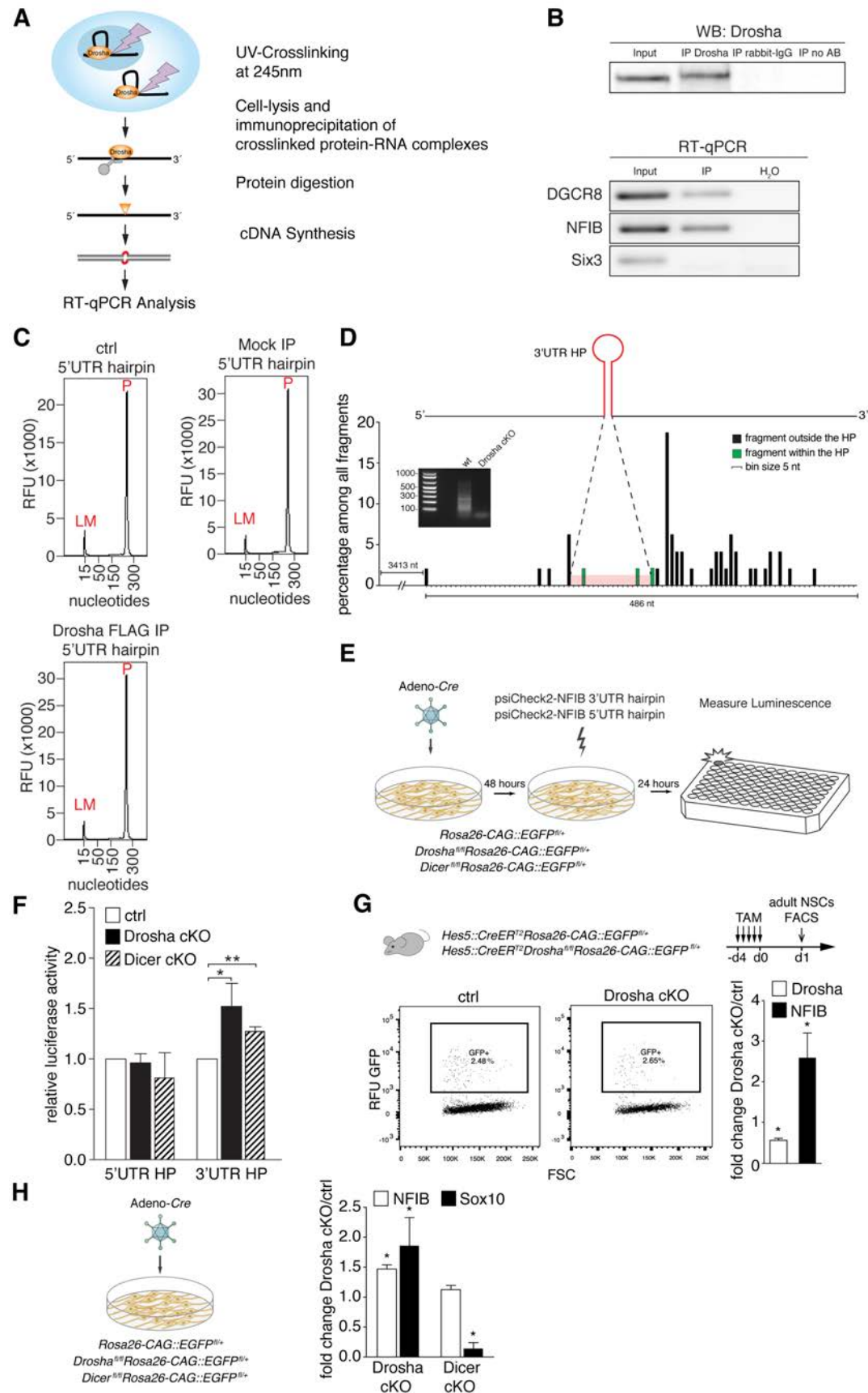


Figure S3. Drosha binds and regulates NFIB mRNA. (A) Scheme of the crosslinked immunoprecipitation (CLIP) procedure. (B) Western-blot for Drosha protein after immunoprecipitation. Rabbit IgG and bead-only (no AB) IPs were performed as negative controls. Drosha CLIP-quantitative RT-PCR for NFIB and DGCR8 (positive control) mRNAs. Six3 mRNA was used as a negative control mRNA in the CLIP experiments. (C) Fragment analyzer electropherograms of NFIB 5'UTR HP RNA probe, control incubated with the beads alone (ctrl) as degradation control, with mock IP, or with flag-tagged Drosha IP (Drosha FLAG IP). Loading marker – LM, full-length probe – P. (D) 5'RACE of NFIB 3'UTR mRNA in wild-type NSCs. Agarose gel of 5'RACE products of control and Drosha cKO NSCs. The diagram represents cleaved fragments identified by Sanger sequencing. Green and black bars identify respectively fragments within and distal to the hairpin sequence. Bin size corresponds to 5 nucleotides. (E) Scheme of luciferase assay. *Rosa26-CAG::EGFP^{fl/+}* (control), *Drosha^{fl/fl}Rosa26-CAG::EGFP^{fl/+}* and *Dicer^{fl/fl}Rosa26-CAG::EGFP^{fl/+}* DG NSCs were infected with adeno-Cre viruses and subsequently transfected with psiCheck-NFIB 5'UTR HP or psiCheck-NFIB 3'UTR HP vectors before quantifying luciferase activity. (F) Relative luciferase activity of the psiCheck2 NFIB 5'UTR HP and 3'UTR HP vectors in control, Drosha cKO and Dicer cKO DG NSCs (Biological replicates $n = 3$. One-sided Student's t-test: $*P < 0.05$, $**P < 0.01$). (G) TAM induction regime for fluorescence activated cell sorting (FACS) of *Hes5::CreER^{T2}*-derived cells. TAM was administered to mice once per day for 5 consecutive days before FACS for GFP⁺ cells at 1 day (d1) after induction. The GFP⁺ population was gated on the basis of the GFP-negative population. Quantitative RT-PCR analysis of Drosha and NFIB mRNA levels in the FACSorted GFP⁺ cells from the Drosha cKO (control $n = 12$, Drosha cKO $n = 19$. Two-sided Student's t-test: $*P < 0.05$). (H) Scheme of the *in vitro* deletion assay. Quantitative RT-PCR analysis of NFIB and Sox10 expression by Drosha cKO and Dicer cKO NSCs 48 hours after adeno-Cre infection (Biological replicates $n = 3$. Two-sided Student's t-test: $*P < 0.05$). Data are mean \pm SEM.

Figure S4, Related to Figure 4

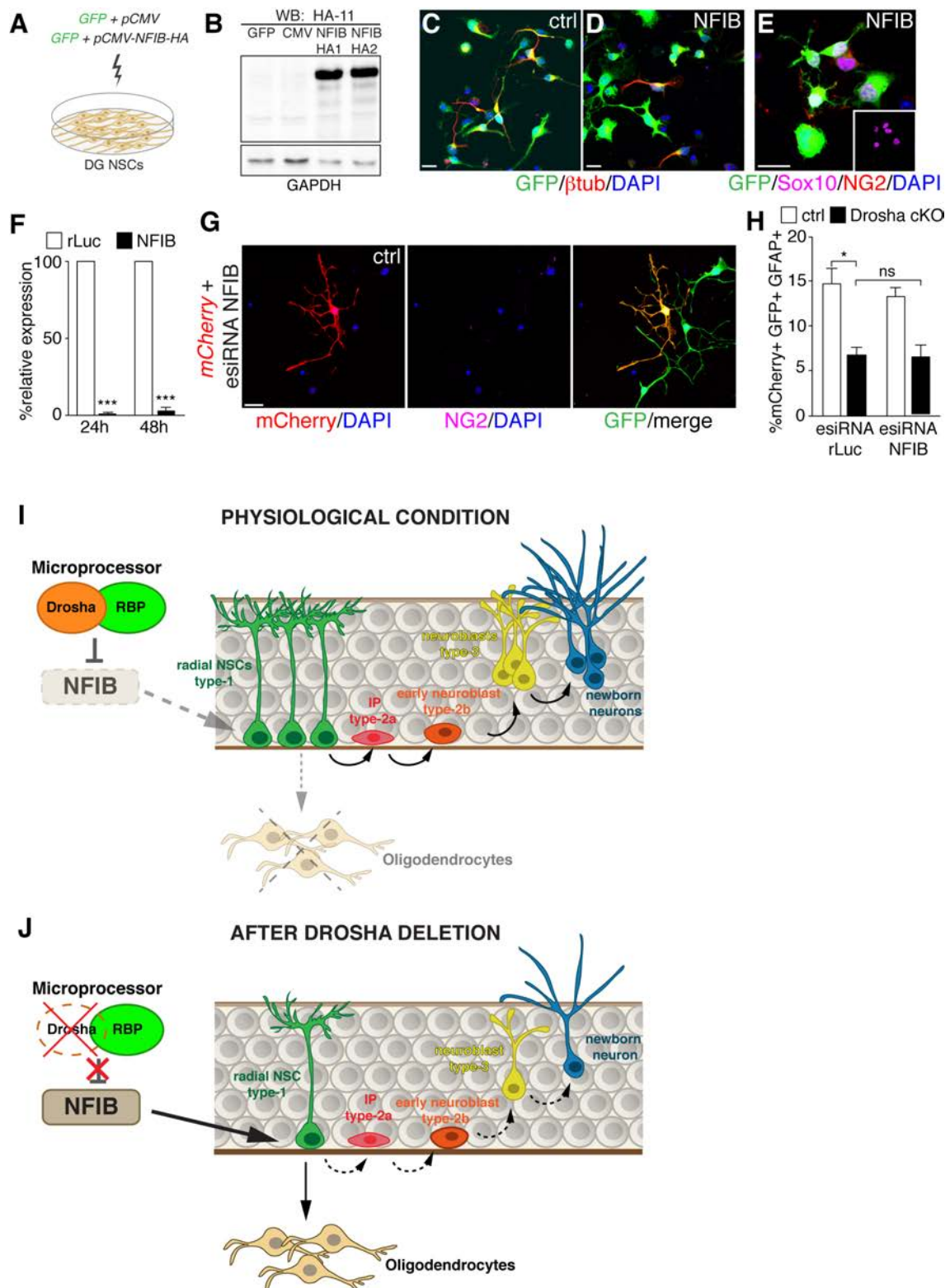


Figure S4. Drosha inhibits oligodendrocyte generation from DG NSCs through NFIB knockdown.

(A) Gain of NFIB function experiments in cultured DG NSCs. pCMV-NFIB or empty pCMV expression vectors were nucleofected into cultured adult DG NSCs. (B) Western-blot analysis of transfected DG NSCs blotted for the HA-tagged NFIB (HA1, HA2 are experimental duplicates) compared to empty pCMV vector (CMV) and pCMV-GFP vector (GFP) only transfected cells. (C-D) β tub expression by pCMV (ctrl: C) and pCMV-NFIB (NFIB: D) transfected DG NSCs after 5 days of differentiation. (E)

Sox10 and NG2 expression by NFIB overexpressing DG NSCs after 5 days of differentiation. (F) Quantitative RT-PCR analysis of N2a cells transfected with the control esiRNA (rLuc) and esiRNA targeting NFIB. NFIB mRNA is not detectable 24 and 48 hours after esiRNA NFIB transfection (Biological replicates $n = 3$. Mann-Whitney test: *** $P < 0.001$). (G) Expression of the oligodendrocyte marker NG2 by control NSCs nucleofected with NFIB esiRNA. (H) Quantification of adeno-Cre infected (GFP⁺), nucleofected mCherry⁺, GFAP⁺ astrocytes in Drosha cKO and control NSCs nucleofected with control esiRNA (rLuc) or NFIB esiRNAs (Biological replicates $n = 3$. Kruskal-Wallis with Dunn post-hoc test: * $P < 0.05$). (I) Under physiological conditions, adult DG NSCs express the RNaseIII Drosha that targets NFIB mRNA and inhibits NFIB protein expression. DG *Hes5*⁺ NSCs (type-1) produce DCX⁺ neuroblasts via intermediate progenitors (IP) that mature into NeuN⁺ granule neurons, but do not generate oligodendrocytes. (J) After Drosha deletion from adult DG NSCs, NFIB mRNA is up regulated. NFIB expression drives NSCs into oligodendrocyte differentiation at the expense of neuron production. RBP, RNA binding protein. Scale bars represent 20 μm in (C), (D), (E) and (G). Data are mean \pm SEM.

Table S1, Related to Figure 1 and S1

Mean \pm SEM (GFP+ cells/mm ²) 5d Tamoxifen + 21d chase					
	GFP+	Sox2+S100 β -	PCNA+	DCX+	radial GFAP+
Control	838.7 \pm 65.3	398.0 \pm 26.1	168.2 \pm 17.8	444.3 \pm 64.6	371.7 \pm 65.5
Drosha cKO	577.5 \pm 46.4	209.0 \pm 34.1	60.5 \pm 16.1	269.5 \pm 34.3	119.4 \pm 30.9
P-values (two-sided t-test)	0.03 (*)	0.01 (*)	0.002 (**)	0.04 (*)	0.02 (*)

Mean \pm SEM (GFP+ cells/mm ²) 5d Tamoxifen + 100d chase					
	GFP+	Sox2+S100 β +	NeuN+	DCX+	radial GFAP+
Control	969.0 \pm 52.4	6.4 \pm 0.4	455.7 \pm 57.5	284.9 \pm 19.1	174.2 \pm 47.7
Drosha cKO	625.3 \pm 23.9	29.8 \pm 1.8	177.3 \pm 51.2	84.9 \pm 19.4	43.2 \pm 17.8
P-values (two-sided t-test)	0.003 (**)	0.002 (***)	0.02 (*)	0.0004 (***)	0.004 (**)

Mean \pm SEM (GFP+ cells/mm ²) 5d Tamoxifen + 21d chase + KA			
	GFP+	DCX+	PCNA+
Control	955.6 \pm 53.8	590.3 \pm 7.7	257.4 \pm 5.4
Drosha cKO	530.0 \pm 40.4	121.4 \pm 15.8	68.2 \pm 10.9
P-values (one-way ANOVA)	0.003 (**)	0.00004 (***)	0.0003 (***)

Table S1: Density of GFP⁺ marker expressing cells in the adult DG *in vivo*. Table showing the density of GFP⁺ cells expressing specific markers at d21 and d100 post-TAM induction and the density of GFP⁺ cells expressing DCX and PCNA d21 after kainic acid (KA) administration in control and Drosha cKO animals. Values are mean \pm SEM.

Table S2, Related to Figure 2

	Mean \pm SEM (GFP+ cells/mm²) adeno-<i>gfap</i>::Cre + 21dpi	
	DCX+	Sox10+
Control	427.8 \pm 85.1	5.3 \pm 2.1
Drosha cKO	141.8 \pm 34.5	127.8 \pm 39.7
Dicer cKO	247.9 \pm 40.7	32.1 \pm 6.4
P-values (one-way ANOVA + Bonferroni Post-Hoc) ctrl vs. Drosha cKO	0.03 (*)	0.0062 (**)
P-values (one-way ANOVA + Bonferroni Post-Hoc) ctrl vs. Dicer cKO	0.2 (ns)	0.5 (ns)
	Sox2+	PCNA+
Control	991.3 \pm 80.4	259.2 \pm 26.0
Drosha cKO	450.3 \pm 116.7	39.3 \pm 22.1
P-values (two-sided t-test)	0.01 (**)	0.003 (**)

Table S2: Density of GFP⁺ marker expressing cells in the adult DG *in vivo* following adeno-*gfap*::Cre adenoviral infection. Table showing the density of GFP⁺ cells expressing specific markers d21 after adeno-*gfap*::Cre adenovirus infection in control and Drosha cKO animals. Values are mean \pm SEM, ns – not significant.

Table S3, Related to Figure 2

	Mean \pm SEM (% GFP+ cells) adeno-Cre + 2 dpi				
	BLBP+	NG2+	β tub+	GFAP+	aCASP3+
Control	47.7 \pm 6.7	0 \pm 0	46.3 \pm 5.1	18.6 \pm 3.4	1.6 \pm 0.8
Drosha cKO	17.4 \pm 5.1	37.7 \pm 7.2	22.1 \pm 2.2	1.6 \pm 1.2	2.4 \pm 1.4
Dicer cKO	42.4 \pm 5.7	4.7 \pm 2.2	23.4 \pm 3.6	16.6 \pm 1.3	4.7 \pm 0.9
P-values (Kruskal-Wallis test) Ctrl vs. Drosha	0.03 (*)	0.001 (**)	0.0029 (**)	0.0011 (**)	0.99 (ns)
P-values (Kruskal-Wallis test) Ctrl vs. Dicer cKO	0.99 (ns)	0.27 (ns)	0.0037 (**)	0.99 (ns)	0.04 (*)

Table S3: Distribution of GFP⁺ marker expressing cells in adult DG NSCs *in vitro* following adeno-Cre-mediated recombination. Table showing the distribution of GFP⁺ cells expressing specific markers 2 days after adeno-Cre adenoviral infection of control, Drosha cKO and Dicer cKO DG NSCs *in vitro*. Values are mean \pm SEM, ns – not significant.

Table S4, Related to Figure 4 and Figure S4

	Mean \pm SEM (% mCherry+GFP+ cells) adeno-Cre + 2 dpi			
	NG2+	BLBP+	β tub+	GFAP+
Control + esiRNA rLuc	2.2 \pm 1.8	47.8 \pm 3.7	46.9 \pm 4.4	14.7 \pm 1.5
Drosha cKO + esiRNA rLuc	64.4 \pm 10	24.6 \pm 2.8	25.6 \pm 2.9	6.7 \pm 0.8
Control + esiRNA NFIB	4.7 \pm 4.7	52.4 \pm 7	46.5 \pm 1.9	13.3 \pm 0.8
Drosha cKO + esiRNA NFIB	23.1 \pm 2.6	48.1 \pm 4.5	45.7 \pm 4.9	6.3 \pm 1.3
P-values (Kruskal-Wallis test)	0.001 (**)	0.006 (**)	0.005 (**)	0.003 (**)

Table S4: Distribution of GFP and mCherry expressing cells in adult DG NSCs following NFIB knockdown *in vitro*. Table showing the distribution of GFP⁺ marker expressing cells after NFIB knockdown and 2 days after adeno-Cre adenoviral infection of control and Drosha cKO DG NSCs *in vitro*. Values are mean \pm SEM.

Supplemental Experimental Procedures

Transgenic animals

Hes5::CreER^{T2}, *Rosa26-CAG::EGFP*, *Drosha^{fl/fl}*, *Dicer^{fl/fl}* mice have been described elsewhere (Chong et al., 2008; Harfe et al., 2005; Lugert et al., 2012; Tchorz et al., 2012). All mice were maintained on a C57BL6 background and were 8-10 weeks old at the onset of the experiments. CreER^{T2}-recombinase activity from the *Hes5CreER^{T2}* locus was induced by Tamoxifen administration (Sigma; 2 mg/injection in corn oil) injected as a single dose intraperitoneal daily for five consecutive days. For *in vivo* clonal analysis animals received one single injection of Tamoxifen (48 mg/kg in corn oil).

Tissue preparation and immunohistochemistry

Mice were deeply anesthetized by injection of a ketamine/xylazine/acepromazine solution (150 mg, 7.5 and 0.6 mg per kg body weight, respectively). Animals were perfused with ice-cold 0.9% saline followed by 4% paraformaldehyde in 0.1M phosphate buffer. Brains were isolated and post-fixed overnight in 4% paraformaldehyde in 0.1M phosphate buffer, and then cryoprotected with 30% sucrose in phosphate buffer at 4°C overnight. Brains were embedded and frozen in OCT (TissueTEK) and sectioned as 30 µm floating sections by cryostat (Leica). Free-floating coronal sections were stored at -20°C in antifreeze solution until use. For clonal analysis, coronal brain sections (45 µm) through the entire dentate gyrus were maintained in series.

Sections were incubated overnight at room temperature, with the primary antibody diluted in blocking solution of 1.5% normal donkey serum (Jackson ImmunoResearch), 0.5% Triton X-100 in phosphate-buffered saline. For clonal analysis, sections were incubated for 48 hours at 4°C, with primary antibody in blocking solution of 1.5% normal donkey serum (Jackson ImmunoResearch), 2% Triton X-100 in phosphate-buffered saline. Antibodies used: AN2 (1:5, gift of Prof. M. Trotter), activated cleavedCASP3 (Cell Signalling, rabbit, 1:500), BLBP (Chemicon, rabbit, 1:500), βtubulinIII (Sigma, mouse, 1:500), DCX (Santa Cruz, goat, 1:500), Drosha (Abcam, rabbit, 1:100), dsRed (Clontech, rabbit, 1:500), GFAP (Sigma, mouse, 1:1000; Santa Cruz, goat, 1:500), GFP (AbD Serotec, sheep, 1:250; Invitrogen, rabbit, 1:700; AvesLabs, chicken, 1:500), NeuN (Millipore, mouse, 1:1000), NG2 (Chemicon, rabbit, 1:500), Olig2 (Millipore, rabbit, 1:500), PCNA (DAKO, mouse, 1:1000), S100β (Sigma, mouse, 1:200), Sox2 (Santa Cruz, goat, 1:500), Sox10 (Santa Cruz, goat, 1:500).

Sections were washed in phosphate-buffered saline and incubated at room temperature for 2 hours with the corresponding secondary antibodies in blocking solution. For clonal analysis sections were incubated for 24 hours at 4°C with the corresponding secondary antibody in blocking solution. Secondary antibodies and detection: Alexa488/Cy3/Alexa555/Alexa594/Alexa647/Alexa649 conjugated anti-chicken, mouse, goat, rabbit, rat and sheep immunoglobulin (1:500, Jackson Immunoresearch). Sections were then washed and counter-stained with DAPI (1 µg/ml). For PCNA and Drosha detection, antigens were recovered at 80 °C for 20 minutes in sodium citrate solution (10 mM, pH7.4). Stained sections were mounted on Superfrost glass slides (Thermo Scientific), embedded in mounting medium containing diazabicyclo-octane (DABCO; Sigma) as an anti-fading agent and visualized using a Zeiss LSM510 confocal microscope, Leica SP5 confocal microscope or Zeiss Apotome2 microscope.

Adeno-*gfap::Cre* adenoviral and retro-*Cre* retrovirus infections in the adult DG

Adult (8-10 week old) mice (*Rosa26-CAG::EGFP^{fl/+}*, *Drosha^{fl/fl}Rosa26-CAG::EGFP^{fl/+}*, *Dicer^{fl/fl}Rosa26-CAG::EGFP^{fl/+}*) were anesthetized in a constant flow of Isoflurane (3%) in oxygen and positioned in a stereotaxic apparatus (David Kopf instruments). Mice were injected with Temgesic subcutaneous (0.05 mg/kg body weight). The skull was exposed by an incision in the scalp and a small hole (1 mm) drilled through the skull. One µl of adeno-*gfap::Cre* adenovirus (titer 1x10¹² infectious particles per ml) or retrovirus-*Cre* (titer 2.7x10⁷, Braun et al., 2015) was injected in the DG using a sharpened borosilicate glass capillaries at the stereotaxic coordinates -2 mm anteroposterior, 1.5 mm lateral to Bregma and -2.0 mm below the surface of the skull. Mice were killed 6, 15 or 21 days after virus infection. Brain tissue was processed and analyzed by immunohistochemistry as described above.

Induction of epileptic seizures

Seizures were induced as described previously (Lugert et al., 2010), kainic acid (KA, Tocris Bioscience) was administered intraperitoneal at 30 mg/kg body weight. Seizures developed within 45 minutes after injection and spontaneously stopped within 2-3 hours. The mice were sacrificed 4 days after KA injection and the brains processed for immunohistochemical analysis as described above.

Hippocampal neural stem cell cultures

Brains of 8-week old *Rosa26-CAG::EGFP^{fl/+}*, *Drosha^{fl/fl}Rosa26-CAG::EGFP^{fl/+}*, *Dicer^{fl/fl}Rosa26-CAG::EGFP^{fl/+}* mice were isolated in L15 Medium (GIBCO) and sectioned live at 300 µm using a

McIlwains tissue chopper. The DG was micro-dissected from the rest of the hippocampus under a dissection binocular microscope avoiding contamination with tissue from the molecular layer, cerebral cortex and subventricular zone, digested in a Papain based solution and mechanically dissociated as described previously (Lugert et al., 2010). Cells were plated in 48-well dishes (Costar) coated with 100 µg/ml Poly-L-Lysine (Sigma) and 1 µg/ml Laminin (Sigma) in neural progenitor culture medium: DMEM:F12 (Gibco, Invitrogen), 2% B27 (Gibco, Invitrogen), FGF2 20 ng/ml (R&D Systems), EGF 20 ng/ml (R&D Systems). DG NSCs were differentiated by growth factor removal and continued culture. Cells were fixed for 10 minutes in 4% paraformaldehyde in 0.1M phosphate buffer and processed as described above.

Adeno-Cre adenovirus infection and AMAXA nucleofection *in vitro*

Rosa26-CAG::EGFP^{fl/+}, *Drosha^{fl/fl}Rosa26-CAG::EGFP^{fl/+}*, *Dicer^{fl/fl}Rosa26-CAG::EGFP^{fl/+}* DG NSCs were transduced with an adeno-Cre adenovirus (titer 1x10¹¹ infectious particles per ml) in growth factor free medium and plated at a density of 5x10⁴ cells/cm² on poly-L-Lysine/Laminin coated coverslips. 48 hours later, the cells were fixed in 4% paraformaldehyde in 0.1M phosphate buffer and process as described above. For western-blot experiments, *Rosa26-CAG::EGFP^{fl/+}*, *Drosha^{fl/fl}Rosa26-CAG::EGFP^{fl/+}*, *Dicer^{fl/fl}Rosa26-CAG::EGFP^{fl/+}* DG NSCs were transduced with an adeno-Cre adenovirus (titer 1x10¹¹ infectious particles per ml) and collected in lysis buffer after 72 hours and processed for western-blot (see below)

Rosa26-CAG::EGFP^{fl/+} and *Drosha^{fl/fl}Rosa26-CAG::EGFP^{fl/+}* adult DG NSC cultures were nucleofected according to the mouse neural stem cell kit instructions (Lonza). Briefly, DG NSCs were dissociated with trypsin and resuspended in the nucleofector solution to a final concentration of 10⁶ cells/100µl. Cell suspensions were combined with either 100 pmol endoribonuclease-prepared siRNAs (esiNA) against NFIB or *Renilla* luciferase (Sigma). *pCAG::mCherry* was added at a ratio 1:3 to identify transfected NSCs. For overexpression, DG NSCs were combined with either pCMV (empty) or pCMV-HA-NFIB (kindly provided by Prof. Heiner Schrewe) vectors and pmaxGFP. NSCs were nucleofected with a Nucleofector 2b device (program A-033). NSCs were immediately transfer to neural progenitor culture medium and plated at the density of 5x10⁴ cells/cm² on poly-L-Lysine/Laminin coated coverslips. 24 hours later, DG NSCs were transduced with an adeno-Cre adenovirus (titer 1x10¹¹ infectious particles per ml) in growth factor free medium and fixed 2 dpi. For overexpression, DG NSCs were fixed 2 days post-nucleofection.

Fluorescence activated cell sorting

Hes5::CreER^{T2}Rosa26-CAG::EGFP^{fl/+} and *Hes5::CreER^{T2}Drosha^{fl/fl}Rosa26-CAG::EGFP^{fl/+}* animals were induced with TAM for five consecutive days and brains collected 1 day after the last injection. NSCs were isolated as described above. Cells were washed with L15 medium (Gibco, Invitrogen), filtered through a 40 µm cell sieve (Miltenyi Biotec) and sorted by forward and side-scatter for live cells (control) and gated for GFP-negative (wild type levels) or GFP⁺ populations with a FACSaria III (BD Biosciences). DAPI (5 mg/ml) was added to discriminate living NSCs. GFP⁺ cells were used for RNA isolation and gene expression analysis (see below).

RNA Isolation and quantitative RT-PCR

Total RNA was isolated using the Trizol method (Life Technologies) and resuspended in water. RNA was treated with RNase-free DNase I (Roche) to remove genomic DNA contamination. First-strand cDNA was generated using BioScript (Bioline) and random hexamer primers followed by quantitative PCR using SensiMix SYBR kit (Bioline). Expression analysis of genes of interest was performed on a Rotor-Gene Q (Qiagen). Primers for quantitative RT-PCR were:

NFIB (Forward: CAGGAGCAAGATTCTGGAC; Reverse: GGGTGTCTTGATACTCTCAC);
NFIB 3'UTR HP (Forward: TAAGTCCTTCAGCCCTTGA ; Reverse: CTGAGGAGGCTGCAGCTAAG)

Sox10 (Forward: AGCTCTGGAGGTTGCTGAAC; Reverse: GCCGAGGTTGGTACTTGTAGTC);
Drosha Exon9-10 (Forward: GACGACGACAGCACCTGTT; Reverse: GATAAATGCTGTGGCGATT);

DGCR8 (Forward: GGAGCTAGATGAAGAAGGAACAGG; Reverse: GTAAAGCGTCCACATCATGTCAA);

Six3 (Forward: TCAGCAGAGTCACGTCAC; Reverse: TGGAGGTTACCGAGAGGATCG)

βactin (Forward: AGGTGACAGCATTGCTTCTG; Reverse: GGGAGACCAAAGCCTTCATA)

Analysis of miRNA expression

Total RNA was isolated from adeno-Cre adenovirus infected *Rosa26-CAG::EGFP^{fl/+}*, *Drosha^{fl/fl}Rosa26-CAG::EGFP^{fl/+}*, *Dicer^{fl/fl}Rosa26-CAG::EGFP^{fl/+}* DG NSCs at 2 dpi using the mirVANA isolation kit following the miRNA enrichment procedure. miRNA profiling was performed on TaqMan arrays (Life

Technologies) with 500 ng of purified RNA according to manufacturer's instructions. Expression analysis was performed using the comparative cycle threshold (Ct) values.

Crosslinking and immunoprecipitation

N2a cells (ATCC) were transfected using Transfectin Lipid Reagent (BioRad) according to manufacturer's instructions with p3X-FLAG-CMV (Sigma) or pCK-Drosha-WT-FLAG (Han et al., 2009; Knuckles et al., 2012) together with psiCheck2 vectors containing the NFIB hairpins. The transfected cells were trypsinized and collected after 48 hours. The mouse NFIB 5' and 3' untranslated regions of 200bp fragments containing the hairpins were amplified by PCR and cloned into the NotI site of psiCheck2 vector (Promega). The cells were cross-linked with 0.5% paraformaldehyde in PBS for 10 minutes, the reaction was quenched by adding Glycine to a final concentration of 140 mM and the cells were lysed by sonication (10 pulses for 10 seconds). Immunoprecipitation was performed for 2 hours at 4°C using anti-Flag M2 Affinity Gel (Sigma-Aldrich). After washing with lysis buffer, the complexes were reverse cross-linked at 70°C for 1 hour. RNA was extracted using Trizol reagent (Invitrogen) according to the manufacturer's instructions and processed as described above.

Primers: psiCheck2 (Forward: TGATCGGAATGGGTAAGTCC; Reverse: GGCCTTGATCTTGTCTTGGT).

Luciferase Assay

Rosa26-CAG::EGFP^{fl/+}, *Drosha^{fl/fl}Rosa26-CAG::EGFP^{fl/+}* and *Dicer^{fl/fl}Rosa26 CAG::EGFP^{fl/+}* DG NSCs were transduced with adeno-Cre or adeno-GFP adenoviruses (see Adeno-Cre infection). 48 hours later, the NSCs were nucleofected with the psiCheck2 containing the 3'UTR or 5'UTR NFIB hairpins (see Crosslinking and Immunoprecipitation) using the AD1 Primary Cell 4D-Nucleofector Y Kit (Lonza) and program EH158. 24 hours post-nucleofection, luciferase activity was measured in a Centro LB 960 Microplate Luminometer (Berthold) using the Dual-Luciferase Reporter Assay System (Promega).

Endogenous CLIP in DG NSCs

A confluent 10 cm dish of DG NSCs was cross-linked at 254 nm at 300 mJ/cm² in a BioLink UV-Crosslinker. Cells were lysed with RIPA buffer (0.1M sodium phosphate pH 7.2, 150 mM sodium chloride, 0.1% SDS, 1% sodium deoxycholate, 1% NP-40) containing complete protease inhibitor cocktail (Roche) and afterwards treated with RNase-free DNase I (Roche). Immunoprecipitation was performed with Protein G Sepharose 4 Fast Flow (GE Healthcare Life Science). Rabbit anti-Drosha Antibody (1:200; D28B1; Cell Signaling) was coupled to the beads for 1 hour at RT, beads were washed three times with RIPA and immunoprecipitation was performed for 2 hours at 4°C. After washing the beads with RIPA buffer, the proteins were digested with 4 mg/ml recombinant PCR grade Proteinase K (Roche) for 1 hour at 37°C with shaking at 1000 rpm. First-strand cDNA synthesis and quantitative RT-PCR was performed as above.

Immunoprecipitation and Western-blot

Beads from the endogenous Drosha immunoprecipitation were resuspended in Lämmli-Buffer containing 2-mercaptoethanol, boiled for 5 minutes and collected at 12000 x g for 20 seconds. Protein samples were separated on 10% SDS-polyacrylamide gels and transferred to Immobilon-P membranes (Millipore). Primary antibody rabbit anti-Drosha (1:1000; D28B1, Cell Signaling), as secondary antibody HRP-conjugated anti-rabbit IgG (1:10000; Jackson ImmunoResearch). Detection was by chemiluminescence (ECL, GE Healthcare). To determine Drosha and Dicer protein expression, *Rosa26-CAG::EGFP^{fl/+}*, *Drosha^{fl/fl}Rosa26-CAG::EGFP^{fl/+}*, *Dicer^{fl/fl}Rosa26-CAG::EGFP^{fl/+}* DG NSCs were transduced with adeno-Cre adenovirus. 24 or 72 hours after infection, the cells were lysed in RIPA Buffer. The lysates were incubated 30 minutes on ice and clarified by centrifugation at 13,000 rpm for 20 minutes. Cell pellets were resuspended in Lämmli-Buffer 3X. Equal amount of protein were separated by 8% SDS-polyacrylamide gel and transferred to Immobilon-P membranes (Millipore). Primary antibodies: anti-HA tag (1:1000; mouse, Covance), anti-Dicer (1:300; rabbit, Sigma), anti-Drosha (1:1000; rabbit, Cell Signaling) and anti-GAPDH (6C5) (1:10000; mouse, Calbiochem). Secondary antibodies HRP-conjugated anti-rabbit IgG (1:10000; Jackson ImmunoResearch) and HRP-conjugated anti-mouse IgG (1:10000; Jackson ImmunoResearch). Detection was by chemiluminescence (ECL, GE Healthcare) and quantification by densitometry using ImageJ software (National Institutes of Health, USA).

In vitro processing

In vitro processing experiments were performed as described previously with some adaptations (Lee and Kim, 2007). Briefly, N2a cells were transfected with pCMV Drosha-Flag or pCMV (empty) vectors. One day after transfection, total cell extracts were prepared in lysis buffer (20mM Tris-HCl, pH 7.8, 100mM KCl, 0.2mM EDTA, 20% (v/v) glycerol, 1mM PMSF) by sonication followed by RNaseA (Sigma) and DNaseI (Roche) treatment and centrifugation at 13400 g for 15 minutes. Total extracts were used for

immunoprecipitation in lysis buffer using Dynabead protein G (Life Technologies) coupled to mouse anti-Flag antibody (1:100, Sigma). 30 μ l of the processing reaction were prepared and contained: 15 μ l of beads from Drosha-Flag immunoprecipitated or uncoupled bead fraction, 6.4 mM MgCl₂, 0.75 μ l RNase Inhibitor (Invitrogen) and 0.5-1 μ g RNA probe containing the 5' UTR or 3'UTR NFIB hairpins transcribed with T7 RNA polymerase (NEB). The reaction was carried out at 25°C for 30 minutes. RNA was extracted using phenol/chloroform and subsequently analyzed on a fragment analyzer using the DNF-472 kit (AATI) and the Low Range ssRNA ladder (NEB).

5' RACE

5' RACE experiments were performed on control and Drosha cKO embryonic NSCs according to 5'RACE System for rapid amplification of cDNA ends version 2.0 kit instructions (Invitrogen). 3 μ g of total RNA of control and Drosha cKO NSCs were used. Nested PCR products were cloned into pGEM-T easy vector (Promega) and sequenced by Sanger sequencing (Microsynth). Fragments were aligned to NFIB sequence using DNASTAR Lasergene.

NFIB RT Primer: AGATCTGTCAATACGAGAA

NFIB 1 Primer: GTTTTCCTAGCCTACCTGGCATT

NFIB nested Primer: TGCCTCTTTGTCTCTACGATGC

***In vivo* clonal analysis**

Confocal images were used to confirm GFP⁺ cell identity according to immunohistological and morphological properties. Whole hippocampi were serially imaged. For 3D reconstruction, optical stacks from the entire DG were serially aligned using Reconstruct 1.1.0 software (Fiala, 2005). Reconstructed hippocampi were analyzed with Imaris Software (Bitplane) with the spot detection tool and manually refined to mark single NSC in the DG. Single cell coordinates were obtained and analyzed using an in-house MATLAB script (The MathWorks, Inc.) in order to get the distance to the nearest GFP⁺ cell neighbor (mean: 184.3 \pm 17.2 μ m, at 2 days after Tamoxifen injection).

Supplemental References

Chong, M.M., Rasmussen, J.P., Rudensky, A.Y., and Littman, D.R. (2008). The RNaseIII enzyme Drosha is critical in T cells for preventing lethal inflammatory disease. *J. Exp. Med.* 205, 2005-2017.

Fiala, J.C. (2005). Reconstruct: a free editor for serial section microscopy. *J. Microsc.* 218, 52-61.

Harfe, B.D., McManus, M.T., Mansfield, J.H., Hornstein, E., and Tabin, C.J. (2005). The RNaseIII enzyme Dicer is required for morphogenesis but not patterning of the vertebrate limb. *Proc. Natl. Acad. Sci. U S A* 102, 10898-10903.

Tchorz, J.S., Suply, T., Ksiazek, I., Giachino, C., Cloetta, D., Danzer, C.P., Doll, T., Isken, A., Lemaistre, M., Taylor, V., *et al.* (2012). A modified RMCE-compatible Rosa26 locus for the expression of transgenes from exogenous promoters. *PLoS One* 7, e30011.